7th International Conference on Fatigue Design, Fatigue Design 2017, 29-30 November 2017, Senlis, France

Fatigue assessment of welded joints in API 579-1/ASME FFS-1 2016 - existing methods and new developments

David A. Osage[a], Pingsha Dong[b], Daniel Spring[a] *

[a]E2G | The Equity Engineering Group, Inc., 20600 Chagrin Blvd., Suite 1200, Shaker Heights, 44122, USA
[b]Welded Structures laboratory, Department of Naval Architecture and marine Engineering, University of Michigan, Ann Arbor, MI 49109

Abstract

The 3rd Edition of API 579-1/ASME FFS-1 2016 *Fitness-For-Service* includes a new Part 14 dedicated to fatigue assessment. An important section in this part covers the fatigue assessment of welded joints. In this paper, an overview of the fatigue methods for welded joints is provided and extensions are recommended. First, an overview is given of the classical fatigue method used in the ASME B&PV Code based on smooth bar fatigue curves in conjunction with a fatigue strength reduction factor. In addition, the mesh insensitive structural stress method is outlined using an equivalent stress parameter based on fracture mechanics considerations in conjunction with a master S-N curve based on the analysis of over 2000 high and low cycle S-N test data. The resulting master S-N curve approach is applicable to high cycle fatigue and low cycle fatigue if a Neuber correction is introduced. In this paper, a new structural strain method is presented to extend the early structural stress based master S-N curve method to the low cycle fatigue regime in which plastic deformations can be significant while an elastic core is present. With this new method, some of the inconsistencies of the pseudo-elastic structural stress procedure can be eliminated, such as its use of Neuber's rule in approximating structural strain beyond yield. The earlier mesh-insensitive structural stress based master S-N curve method can now be viewed as an application of the structural strain method in the high cycle regime, in which structural strains are linearly related to traction-based structural stresses according to Hooke's law. Thus, both low cycle and high cycle fatigue behavior can now be treated in a unified manner. In the low-cycle regime, the structural strain method characterizes fatigue damage directly in terms of structural strains that satisfy a linear through-thickness deformation gradient assumption, material nonlinear behavior, and equilibrium conditions. A PVRC Joint Industry Project is currently sponsoring work on the structural strain method that will lead to its incorporation in the next edition of API 579-1/ASME FFS-1.

* Corresponding author. Tel.: +1-216-658-4789; fax: +1-216-283-6022.
  E-mail address: daosage@equityeng.com

1. Introduction

In a previous paper, Osage [1] provides an overview of the third edition of API 579-1/ASME FFS-1 *Fitness-For-Service* that was published in 2016. The 2016 Edition includes a new Part 14 covering fatigue assessment procedures for in-service components. Fitness-For-Service (FFS) assessments are quantitative engineering evaluations that are performed to demonstrate the structural integrity of an in-service component that may contain a flaw or damage, or that may be operating under a specific condition that might cause a failure. The API 579-1/ASME FFS-1 Standard was specifically written to cover in-service pressurized equipment typically found in the refining and petrochemical industries as well as the fossil utility industry. Part 14 provides methods used to estimate the time to crack initiation using a strain-life approach and is written as a multi-level approach covering screening, current design code methods, and advanced methods that take into account the latest in technology. The advanced methods include fatigue assessment of welded joints using the equivalent structural strain and Master S-N Curve Method and a new smooth-bar fatigue assessment method that incorporates a multi-axial fatigue criterion with a critical plane approach. Cycle counting methods for both welded joint and smooth-bar fatigue methods are also provided. Methods to evaluate fatigue in the subcritical crack-growth regime in API 579-1/ASME FFS-1 using a fracture mechanics approach are also covered.

In this paper, an overview is given of the fatigue analysis methods in Part 14 of API 579-1/ASME FFS-1 2016, pertaining to the assessment of welded joints, as listed below. The fatigue analysis of welded joints may be performed using smooth bar fatigue curve methods or fatigue analysis methods based on welded joint fatigue curves. Cycle counting and plasticity correction procedures are provided for each method in reference [2].

- Level 2, Method A – Fatigue assessment using elastic stress analysis and equivalent stresses: the fatigue damage and remaining life are computed based on an effective total equivalent stress obtained from a linear elastic stress analysis, and a smooth bar fatigue curve.
- Level 2, Method B – Fatigue assessment using elastic-plastic stress analysis and equivalent strain: the fatigue damage and remaining life are computed based on an effective strain range obtained from an elastic-plastic stress analysis, and a smooth bar fatigue curve.
- Level 2, Method C – Fatigue assessment of welds using the equivalent structural stress: the fatigue damage and remaining life are computed based on an equivalent structural stress range parameter obtained from a linear elastic stress analysis, and a welded joint fatigue curve.
- Level 3 – Fatigue assessment using elastic or elastic-plastic stress analysis and shear and normal strains: a multiaxial strain-life method is used with a critical plane approach. Fatigue damage is calculated on each candidate plane using a strain-life equation, the plane with the maximum damage identifies the critical plane and the overall fatigue damage for a given point. The strain-life equation is based on Brown-Miller adjusted for mean stress effects.

A new structural strain method is presented to extend the early structural stress based master S-N curve method to the low cycle fatigue regime in which plastic deformations can be significant while an elastic core is present. The loading conditions which satisfy this criteria are derived via the Bree diagram. In the late 1960's, Bree developed a theory and corresponding diagram plotting the primary membrane stress versus the cyclic thermal stress which delineates the various zones of plastic behavior. The zones include elastic cycling, plastic cycling, elastic cycling after initial plasticity, and ratcheting leading to incremental growth. In this paper, the Bree diagram is extended to four different cyclic loading cases that also account for the ratio of the yield stress at the operating extremums of the cycle. These four cyclic loading cases can be used to determine the appropriate structural stress range to be used in a fatigue assessment using the structural strain method.

The new structural strain method is then presented to extend the early structural stress based master S-N curve method, i.e. Level 2 Method C, to the low cycle fatigue regime in which plastic deformation can be significant

while an elastic core is still present. The method is formulated by taking advantage of elastically calculated mesh-insensitive structural stresses based on nodal forces available from finite element solutions. The structural strain definition is consistent with classical plate and shell theory in which a linear through-thickness deformation field is assumed a priori in the elastic or elastic-plastic regimes. With considerations of both yield and equilibrium conditions, the resulting structural strains are analytically solved under plane-stress conditions, assuming elastic and perfectly plastic material behavior. Numerical solutions will be provided for plane strain conditions and a Ramberg-Osgood stress-strain relationship [3]. The method is shown effective in correlating low-cycle fatigue test data of various sources documented in the literature into a single narrow scatter band which is remarkably consistent with the scatter band of the existing master S-N curve adopted by the ASME B&PV Code since 2007 [4]. With this new method, some of the inconsistencies of the existing pseudo-elastic structural stress procedure, Level 2 Method C, can now be eliminated, such as its use of Neuber's rule in approximating structural strain beyond yield. More importantly, both low cycle and high cycle fatigue behavior can now be treated in a unified manner. The earlier mesh-insensitive structural stress based master S-N curve method can now be viewed as an application of the structural strain method in the high cycle regime, in which structural strains are linearly related to traction-based structural stresses according to Hooke's law. In the low-cycle regime, the structural strain method characterizes fatigue damage directly in terms of structural strains that satisfy a linear through-thickness deformation gradient assumption, material nonlinear behavior, and equilibrium conditions. In addition, a step-by-step procedure is provided to illustrate how the ratcheting rules based on elastic stress analysis can be treated in an integrated manner using the structural strain method for differentiating axial growth related damage from fatigue damage for incorporation in the existing equivalent structural stress approach in API 579-1/ASME FFS-1, 2016 Edition.

Nomenclature

a	depth of a crack at the weld toe.
b	extent of plasticity through the cross section.
C	welded joint fatigue curve coefficient.
c	size of the elastic core
b_k	exponent in Brown-Miller strain-life equation.
b_k	exponent in Brown-Miller strain-life equation.
c_k	exponent in Brown-Miller strain-life equation.
$\Delta e_{ij,k}$	change in elastic strain range at the point under evaluation for the kth cycle.
$\Delta \varepsilon_k$	local nonlinear structural strain range at the point under evaluation for the kth cycle.
$\Delta \varepsilon_{peq,k}$	equivalent plastic strain range for the kth loading condition or cycle.
$\Delta \varepsilon_k^e$	elastically calculated structural strain range at the point under evaluation for the kth cycle.
$\Delta \varepsilon_{eff,k}$	effective strain range for the kth cycle.
$\Delta \varepsilon_{e,k}$	equivalent elastic strain range for the kth loading condition or cycle.
$\Delta \varepsilon_{peq,k}$	equivalent plastic strain range for the kth loading condition or cycle.
$\Delta \varepsilon_{N,k}$	normal strain range on the critical plane for the kth cycle.
$\Delta \gamma_k$	shear strain range on the critical plane for the kth cycle.
$\Delta p_{ij,k}$	change in plastic strain range at the point under evaluation for the kth cycle.
$\Delta S_{P,k}$	range of primary plus secondary plus peak equivalent stress for the kth cycle.

$\Delta S_{ess,k}$	range of equivalent structural stress for the kth cycle.
$\Delta \sigma_k$	structural stress range at the point under evaluation for the kth cycle.
$\Delta \sigma_{ij,k}$	stress tensor range at the point under evaluation for the kth cycle.
$\Delta \sigma_k^e$	elastically calculated structural stress range at the point under evaluation for the kth cycle.
$\Delta \sigma_{b,k}^e$	elastically calculated structural bending stress range at the point under evaluation for the kth cycle.
$\Delta \sigma_{m,k}^e$	elastically calculated structural membrane stress range at the point under evaluation for the kth cycle.
$\Delta \tau_k^e$	elastically calculated shear stress range at the point under evaluation for the kth cycle.
$\Delta \tau_{b,k}^e$	elastically calculated shear bending stress range at the point under evaluation for the kth cycle.
$\Delta \sigma_{m,k}^e$	elastically calculated shear membrane stress range at the point under evaluation for the kth cycle.
E	modulus of elasticity.
E'	modulus of elasticity for plane strain.
E_{ACS}	modulus of elasticity of carbon steel at ambient temperature or 21°C (70°F).
E_T	modulus of elasticity of the material under evaluation at the average temperature of the cycle.
E_y	modulus of elasticity at the temperature of interest.
E_{yf}	value of modulus of elasticity on the fatigue curve being utilized.
$E_{ya,k}$	value of modulus of elasticity evaluated at the mean temperature of the kth cycle.
e	distance from the centerline to the neutral axis.
ε	strain.
ε_i	strain at the inner fiber of the cross section.
ε_o	strain at the outer fiber of the cross section.
$\varepsilon_{f,k}'$	strain-life equation parameter for the kth cycle.
F	peak equivalent stress.
$F(\delta)$	fatigue modification factor based on the out-of-phase angle between $\Delta \sigma_k$ and $\Delta \tau_k$.
f_E	environmental correction factor to the welded joint fatigue curve.
f_I	fatigue improvement method correction factor to the welded joint fatigue curve.
f_{MT}	material and temperature correction factor to the welded joint fatigue curve.
f_e	environmental knock-down factor for fatigue.
f_I	fatigue improvement factor
$f_{M,k}$	mean stress correction factor for the kth cycle.
h	welded joint fatigue curve exponent.
I	correction factor used in the structural stress evaluation.
K_{css}	parameter for the cyclic stress-strain curve.
$K_{e,k}$	fatigue penalty factor for the kth cycle

m_{ss}	exponent used in a fatigue analysis based on the structural stress.
$N_{f,k}$	number of cycles to failure for the kth cycle.
n_{css}	material parameter for the cyclic stress-strain curve model.
ν	poisson's ratio.
P_b	primary bending equivalent stress.
P_L	local primary membrane equivalent stress.
P_m	general primary membrane equivalent stress.
q	parameter to determine the effect equivalent structural stress range on the fatigue improvement factor.
Q	secondary equivalent stress.
R	ratio of the hot to cold yield stresses or the radius of curvature.
R_k	stress ratio for the kth cycle.
$R_{b,k}$	ratio of the bending stress to the membrane plus bending stress for the kth cycle.
$R_{b\tau,k}$	ratio of the bending shear stress to the membrane plus bending shear stress for the kth cycle.
S	allowable primary stress.
S_a	allowable cyclic stress established from a fatigue curve.
$S_{alt,k}$	alternating equivalent stress for the kth cycle.
S_{ps}	allowable primary plus secondary stress.
S_y	yield strength.
S'_y	yield strength for plane strain.
$S_{y,k}$	yield strength of the material evaluated at the mean temperature of the kth cycle.
σ_1	stress used to derive the structural strain for one-sided yield condition.
$\sigma_{max,k}$	maximum stress for the kth cycle.
$\sigma_{min,k}$	minimum stress for the kth cycle.
$\sigma_{N-mean,k}$	normal mean stress on the critical plane in the kth cycle.
σ_{y-cold}	yield strength at the cold part of the cycle.
σ_{y-hot}	yield strength at the hot part of the cycle.
σ_{ys}	yield strength at the assessment temperature.
σ'_b	elastic bending stress.
σ'_m	elastic membrane stress.
σ_p	primary membrane stress.
σ_{ss}	secondary bending stress.
σ'_i	pseudo elastic stress at the inner fiber of the cross section.
σ'_b	pseudo elastic bending stress.

σ'_m	pseudo elastic membrane stress.
σ'_o	pseudo elastic stress at the outside fiber of the cross section.
$\sigma'_{f,k}$	strain-life equation parameter for the kth cycle.
${}^m\sigma^e_{m,k}$	yield strength at the assessment temperature.
${}^m\sigma^e_{b,k}$	elastically calculated bending stress normal to the hypothetical crack plane at the location under evaluation at time point ${}^m t$ for the kth cycle.
${}^n\sigma^e_{b,k}$	elastically calculated bending stress normal to the hypothetical crack plane at the location under evaluation at time point ${}^n t$ for the kth cycle.
${}^m\sigma^e_{m,k}$	elastically calculated membrane stress normal to the hypothetical crack plane at the location under evaluation at time point ${}^m t$ for the kth cycle.
${}^n\sigma^e_{m,k}$	elastically calculated membrane stress normal to the hypothetical crack plane at the location under evaluation at time point ${}^n t$ for the kth cycle.
t	thickness.
t_{ess}	equivalent structural stress effective thickness.
${}^m\tau^e_{b,k}$	elastically calculated bending component of shear stress parallel to the hypothetical crack plane at the location under evaluation at time point ${}^m t$ for the kth cycle.
${}^n\tau^e_{b,k}$	elastically calculated bending component of shear stress parallel to the hypothetical crack plane at the location under evaluation at time point ${}^n t$ for the kth cycle.
${}^m\tau^e_{m,k}$	elastically calculated membrane component shear stress parallel to the hypothetical crack plane at the location under evaluation at time point ${}^m t$ for the kth cycle.
${}^n\tau^e_{m,k}$	elastically calculated membrane component shear stress parallel to the hypothetical crack plane at the location under evaluation at time point ${}^n t$ for the kth cycle.
X	parameter used for the abscissa of the Bree diagram.
y	local coordinate through the distance of the cross section.
Y	parameter used for the ordinate of the Bree diagram.

2. Fatigue of Welded Joints in API 579-1/ASME FFS-1

2.1. Overview

The fatigue analysis methods in API 579-1/ASME FFS-1 are illustrated in Figure 1. Each of these methods may be used for the analysis of welded joints. A summary of each method and how it is used for the analysis of welded joints is provided in the following paragraphs. In the description of the methods for fatigue that follow, each method is summarized based on a driving force and resistance concept. The driving force is the alternating stress or strain amplitude or Equivalent Structural Stress range from the fatigue loading. It is the parameter that drives the fatigue damage. The resistance is the allowable number of cycles from a fatigue curve.

Figure 1. Fatigue analysis methods in API 579-1/ASME FFS-1

2.2. Level 2 – Method A: Equivalent Stress Range and Smooth Bar Fatigue Curve

The technical basis and methodology for Level 2, Method A is provided in reference [5]. This method represents the original fatigue design method incorporated into the ASME B&PV Code, Section VIII, Division 2 and remains essentially unchanged since its original publication in 1968. The main issue in using this method for the fatigue analysis of welded joints is that the stress results are sensitive to the mesh density of the finite element model. Numerous methods have been introduced to overcome this sensitivity such as the use of a hot-spot stress or a fatigue strength reduction factor; however, considerable variability in analysis results still remains.

2.2.1. Driving Force

In the Level 2 Method A procedure, the effective total equivalent stress amplitude is used to evaluate the fatigue damage for results obtained from a linear elastic stress analysis. The controlling stress for the fatigue evaluation is the primary plus secondary plus peak equivalent stress amplitude that is defined as one-half of the primary plus secondary plus peak stress equivalent stress range, (P_L+P_b+Q+F), calculated for each cycle in the loading history. Figure 2 taken from API 579-1/ASME FFS-1, is a graphical representation of the stress calculations and classifications used with a linear elastic stress analysis. The primary plus secondary plus peak stress equivalent stress range is the equivalent stress, derived from the highest value across the thickness of a section, of the combination of all primary, secondary, and peak stresses produced by specified operating pressures and other mechanical loads and by general and local thermal effects and including the effects of gross and local structural discontinuities.

Stress Category	Primary			Secondary Membrane plus Bending	Peak
	General Membrane	Local Membrane	Bending		
Description (see Annex 2D and VIII-2, Part 5)	Average primary stress across solid section. Excludes dis-continuities and concentrations. Produced only by mechanical loads.	Average stress across any solid section. Considers dis-continuities but not concentra-tions. Produced only by mech-anical loads.	Component of primary stress proportional to distance from centroid of solid section. Excludes dis-continuities and concentrations. Produced only by mechanical loads.	Self-equilibrating stress necessary to satisfy contin-uity of structure. Occurs at struc-tural discontinui-ties. Can be caused by mechanical load or by differential thermal expansion. Excludes local stress concentrations.	1. Increment added to primary or secondary stress by a concentration (notch). 2. Certain ther-mal stresses which may cause fatigue but not distor-tion of vessel shape.
Symbol	P_m	P_L	P_b	Q	F

Figure 2. Hopper Diagram for stress calculations and classifications to be used with a linear elastic stress analysis

The Method A procedure represents the ASME fatigue design method developed in the 1960's that has survived basically unaltered. The procedure was updated in 2007 to calculate the alternating stress amplitude for the kth cycle using component stress differences as shown below. The plasticity correction factor in this equation, $K_{e,k}$, is fully described in reference [5] and remains unchanged after 50 years.

$$S_{alt,k} = \frac{K_{e,k} \cdot \Delta S_{P,k}}{2} \qquad (1)$$

$$\Delta S_{P,k} = \frac{1}{\sqrt{2}} \left[\begin{array}{l} \left(\Delta\sigma_{11,k} - \Delta\sigma_{22,k}\right)^2 + \left(\Delta\sigma_{11,k} - \Delta\sigma_{33,k}\right)^2 + \\ \left(\Delta\sigma_{22,k} - \Delta\sigma_{33,k}\right)^2 + 6\left(\Delta\sigma_{12,k}^2 + \Delta\sigma_{13,k}^2 + \Delta\sigma_{23,k}^2\right) \end{array} \right]^{0.5} \qquad (2)$$

For implementation of this method into API 579-1/ASME FFS-1, it was decided not to alter the method for computing the alternating stress amplitude. However, a new multiaxial cycle counting routine has been added to identify the kth cycles for variable amplitude loading [2].

The effect of the weldment is typically accounted for by introducing a fatigue strength reduction factor, K_f, into the stress range calculation, or

$$\Delta S_{P,k} = \frac{1}{\sqrt{2}} \left[\begin{array}{l} \left(\Delta\sigma_{11,k} - \Delta\sigma_{22,k}\right)^2 + \left(\Delta\sigma_{11,k} - \Delta\sigma_{33,k}\right)^2 + \\ \left(\Delta\sigma_{22,k} - \Delta\sigma_{33,k}\right)^2 + 6\left(\Delta\sigma_{12,k}^2 + \Delta\sigma_{13,k}^2 + \Delta\sigma_{23,k}^2\right) \end{array} \right]^{0.5} \tag{3}$$

$$\Delta\sigma_{ij,k} = K_f \cdot \left({}^m\sigma_{ij,k} - {}^n\sigma_{ij,k} \right) \tag{4}$$

Recommendations for fatigue strength reduction factors are provided based on the quality of original code construction methods and examination performed (see Tables 1 and 2).

Table 1. Weld surface fatigue strength reduction factors

Weld Condition	Surface Condition	Quality Levels						
		1	2	3	4	5	6	7
Full penetration	Machined	1.0	1.5	1.5	2.0	2.5	3.0	4.0
	As-welded	1.2	1.6	1.7	2.0	2.5	3.0	4.0
Partial penetration	Final surface machined	NA	1.5	1.5	2.0	2.5	3.0	4.0
	Final surface as-welded	NA	1.6	1.7	2.0	2.5	3.0	4.0
	Root	NA	1.5	NA	NA	NA	3.0	4.0
Fillet	Toe machined	NA	NA	1.5	NA	2.5	3.0	4.0
	Toe as-welded	NA	NA	1.7	NA	2.5	3.0	3.0 - 4.0
	Root	NA	NA	NA	NA	NA	3.0	4.0

Table 2. Weld surface fatigue strength reduction factors

Fatigue-Strength-Reduction Factor	Quality Level	Definition
1.0	1	Machined or ground weld that receives a full volumetric examination, and a surface that receives MT/PT examination and a VT examination.
1.2	1	As-welded weld that receives a full volumetric examination, and a surface that receives MP/PT and VT examination.
1.5	2	Machined or ground weld that receives a partial volumetric examination, and a surface that receives MT/PT examination and VT examination.
1.6	2	As-welded weld that receives a partial volumetric examination, and a surface that receives MP/PT and VT examination.
1.5	3	Machined or ground weld surface that receives MT/PT examination and a VT examination (visual), but the weld receives no volumetric examination inspection.
1.7	3	As-welded weld surface that receives MT/PT examination and a VT examination (visual), but the weld receives no volumetric examination inspection.
2.0	4	Weld has received a partial or full volumetric examination, and the surface has received VT examination, but no MT/PT examination.
2.5	5	VT examination only of the surface; no volumetric examination nor MT/PT examination.
3.0	6	Volumetric examination only.
4.0	7	Weld backsides that are non-definable and/or receive no examination.

Notes:

1. Volumetric examination is RT or UT in accordance with the applicable construction code.

2. MT/PT examination is magnetic particle or liquid penetrant examination in accordance with the applicable construction code.

Table 2. Weld surface fatigue strength reduction factors

Fatigue-Strength-Reduction Factor	Quality Level	Definition
3.		VT examination is visual examination in accordance with the applicable construction code.
4.		See WRC Bulletin 432 for further information.

The effect of the weldment may also be accounted for by introducing an effective notch [6]. The effective notch stress approach considers the increase in local stress at the notch formed by the weld toe or the weld root, based on the theory of elasticity, i.e. without consideration of elastic-plastic material behavior. The micro-structural support effect of the material, which considers the effect of the inhomogeneous material structure under a stress gradient on fatigue behavior, may be taken into account by averaging the stress over a definite area. The basic idea behind this approach is that the stress reduction in a notch due to averaging the stress over a certain depth can alternatively be achieved by a fictitious enlargement of the notch radius, as illustrated in Figure 3. A fictitious radius of $R_{eff} = 1$ mm, termed reference radius has been shown to be conservative. This reference radius, derived for welded joints in steel, is also used for welded joints in aluminum and magnesium alloys.
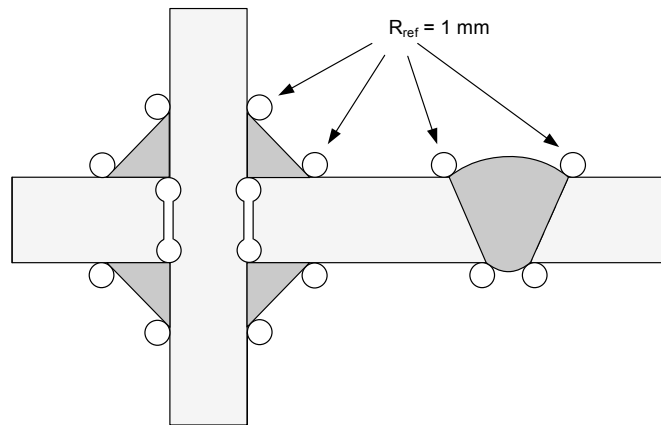
Figure 3. Fatigue analysis using an effective notch

Another method that has been used to neutralize the stress singularity effect associated with a weld toe is the hot spot stress approach [7]. The hot spot stress approach for fatigue analysis is applicable only to situations where the potential mode of failure is by fatigue crack growth from the toe of a weld. The method may be used either with shell or solid elements. The method uses stress results at prescribed distances from the weld toe, two or three points may be used. The hot spot stress at the weld toe is subsequently obtained by linear or quadratic extrapolation of these stress results to the weld toe. While the method does resolve the issue of a stress singularity at the weld toe it has been shown to be mesh dependent [8-9]. Therefore, the International Institute for Welding (IIW) has issued guidelines [6] for element size and equations for extrapolation to obtain consistency in fatigue analysis results (see Tables 3-4 and Figure 4).

Table 3. IIW recommended meshing and extrapolation for computation of the hot spot stress

Type of Model and Weld Toe		Relatively Course Mesh		Relatively Fine Mesh	
		Type A	Type B	Type A	Type B
Element Size	Shells	$t \, x \, t$ with max $t \, x \, w/2$ (1)	$10 \, x \, 10 \, mm$	$\leq 0.4txt$ or $\leq 0.4tx \, w/2$	$\leq 4x4 \, mm$
	Solids	$t \, x \, t$ with max $t \, x \, w$	$10 \, x \, 10 \, mm$	$\leq 0.4txt$ or $\leq 0.4tx \, w/2$	$\leq 4x4 \, mm$
Extrapolation Points	Shells	$0.5t$ and $1.5t$ midside points (2)	5 and $15 \, mm$ midside points	$0.4t$ and $1.0t$ nodel points	$4, 8,$ and $12 \, mm$ nodel points
	Solids	$0.5t$ and $1.5t$ surface center	5 and $15 \, mm$ surface center	$0.4t$ and $1.0t$ nodel points	$4, 8,$ and $12 \, mm$ nodel points

Notes:

1. w is the longitudinal attachment thickness plus 2 weld leg lengths

2. Surface center at transverse welds, if the weld below the plate is not modelled

Table 4. IIW recommended meshing and extrapolation equations for calculation of the hot spot stress

Type	Description	Equation
A	Fine mesh with an element length not more than 0.4t at the hot spot. Evaluation of nodal stresses at two reference points 0.4t and 1.0t, and linear extrapolation	$\sigma_{HS} = 1.67 \cdot \sigma_{0.4t} - 0.67 \cdot \sigma_{1.0t}$
	Fine mesh as defined above. Evaluation of nodal stresses at three reference points 0.4t, 0.9t and 1.4t and quadratic extrapolation. This method is recommended for cases of pronounced non-linear structural stress increase towards the hot spot, at sharp changes of direction of the applied force or for thick-walled structures	$\sigma_{HS} = 2.52 \cdot \sigma_{0.4t} - 2.24 \cdot \sigma_{0.9t} + 0.72 \cdot \sigma_{1.4t}$
	Coarse mesh with higher order elements having lengths equal to the plate thickness at the hot spot. Evaluation of stresses at the mid-side points or surface centers respectively, i.e. at two reference points 0.5t and 1.5t, linear extrapolation.	$\sigma_{HS} = 1.50 \cdot \sigma_{0.5t} - 0.50 \cdot \sigma_{1.5t}$
B	Fine mesh with element length of not more than 4 mm at the hot spot. Evaluation of nodal stresses at three reference points 4 mm, 8 mm and 12 mm, and quadratic extrapolation	$\sigma_{HS} = 3.0 \cdot \sigma_{4mm} - 3.0 \cdot \sigma_{8mm} + \sigma_{12mm}$
	Course mesh with higher order elements having a length of 10 mm, at the hot spt. Evaluation of stresses at the mid-side points of the first two elements and linear extrapolation.	$\sigma_{HS} = 1.5 \cdot \sigma_{5mm} - 0.5 \cdot \sigma_{15mm}$

Notes:

1. w is the longitudinal attachment thickness plus 2 weld leg lengths

2. Surface center at transverse welds, if the weld below the plate is not modelled

Definition of Type A and B Hot Spots

Figure 4. IIW Definition and extrapolation recommendations
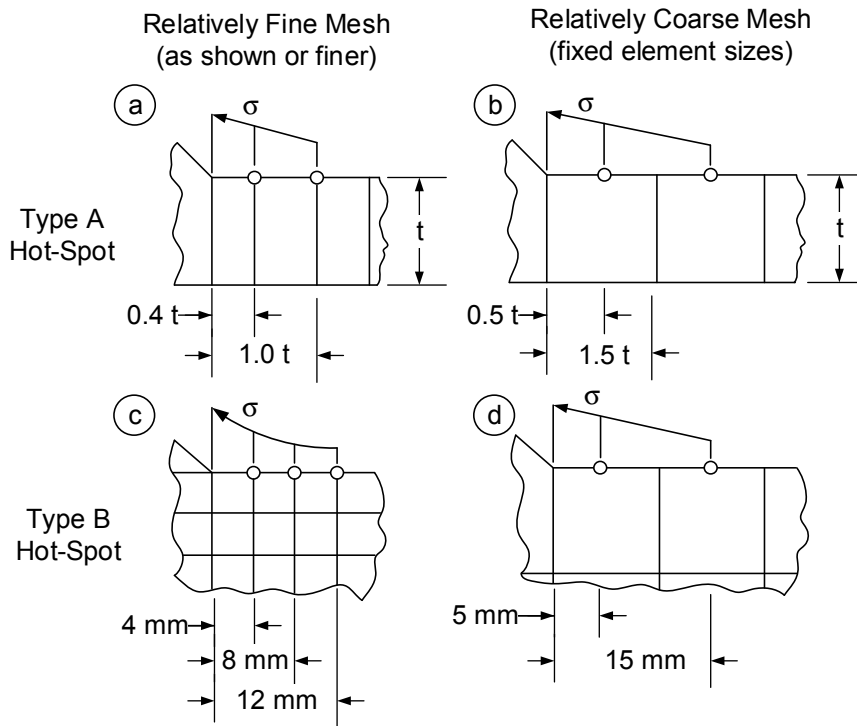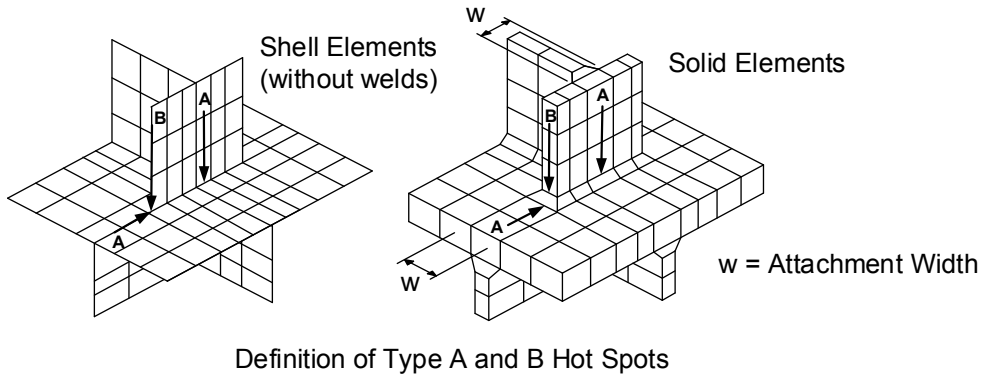
It should be noted that the mesh density required for the effective notch and hot spot approach is much larger than that required for the equivalent structural stress approach. The increase in the mesh density required for a solution may add significant time to the analysis especially if multiple cases need to be examined.

2.2.2. Resistance

The fatigue curve used to determine the permissible number of cycles is based on smooth bar test results and is shown in Figure 5. This fatigue curve is applicable to carbon, low alloy, series 4xx, high alloy steels, and high tensile strength steels for temperatures not exceeding 371°C. The cusp in the curve at approximately 10,000 cycles is a result of the design margins included in the curve. The design margin for each point on the curve is set based on taking the minimum of the stress amplitude divided by two and the number of cycles divided by 20. The factor of 20 on cycles is the product of the following sub-factors [5].

- Scatter of data (minimum to mean)   –   2.0
- Size effect   –   2.5
- Surface finish, atmospheric, etc. –   –   4.0
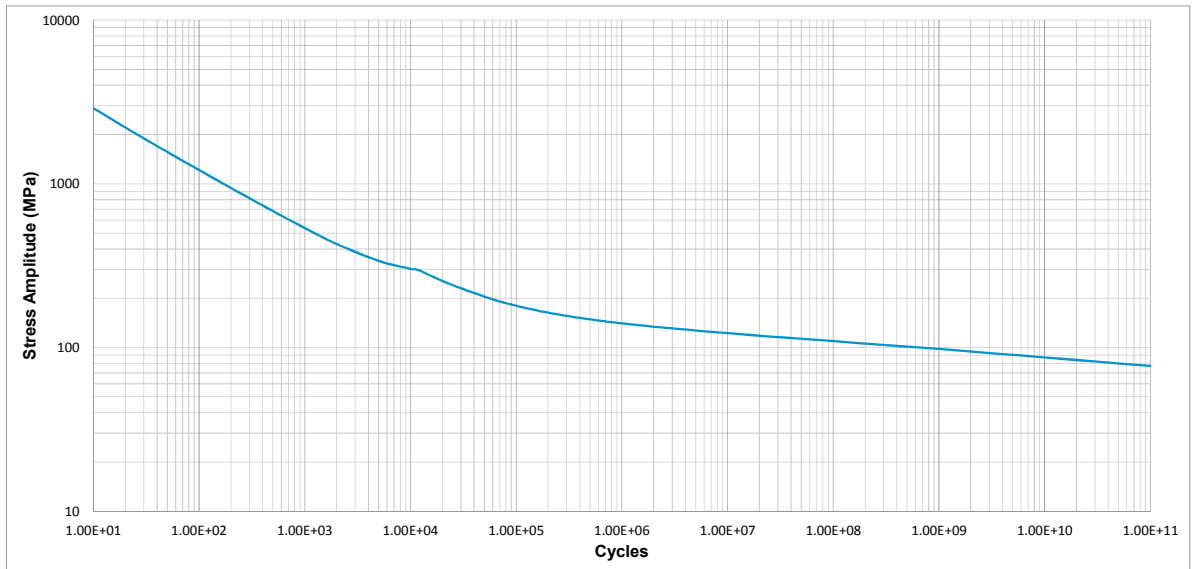
Figure 5. Level 2, Method A and Method B fatigue curve based on smooth bar test results

2.3. Level 2 – Method B: Equivalent Strain Range and Smooth Bar Fatigue Curve

The technical basis and methodology for Level 2, Method B is provided in reference [5]. This method was introduced into the 2007 Edition of the ASME B&PV Code, Section VIII, Division 2 in 2007. Level 2, Method B is the strain-based version of Level 2, Method A, i.e. elastic-plastic analysis is used to compute the total strain range directly as opposed to approximating it from an elastic analysis. While this method is computationally intensive, it is general and gaining more use because of the CPU speed of modern day computing. As with Level 2, Method A, the main issue using this method for the fatigue analysis of welded joints is that the stress results are sensitive to the mesh density of the finite element model.

2.3.1. Driving Force

In Method B, an effective strain range is used to evaluate the fatigue damage based on the results from an elastic-plastic stress analysis. This analysis is performed for the complete loading time history using a cyclic plasticity algorithm with kinematic hardening. The effective strain range is calculated using the equation shown below for the kth cycle identified using a multiaxial cycle counting procedure as described in reference [5].

$$S_{alt,k} = \frac{E_{yf} \cdot \Delta\varepsilon_{eff,k}}{2} \tag{5}$$

$$\Delta\varepsilon_{eff,k} = \Delta\varepsilon_{e,k} + \Delta\varepsilon_{peq,k} \tag{6}$$

$$\Delta\varepsilon_{e,k} = \frac{1}{\sqrt{2}} \left[\begin{array}{l} \left(\Delta e_{11,k} - \Delta e_{22,k}\right)^2 + \left(\Delta e_{22,k} - \Delta e_{33,k}\right)^2 + \\ \left(\Delta e_{33,k} - \Delta e_{11,k}\right)^2 + 6\left(\Delta e_{12,k}^2 + \Delta e_{23,k}^2 + \Delta e_{31,k}^2\right) \end{array} \right]^{0.5} \tag{7}$$

$$\Delta\varepsilon_{peq,k} = \frac{\sqrt{2}}{3}\left[\begin{array}{c}\left(\Delta p_{11,k} - \Delta p_{22,k}\right)^2 + \left(\Delta p_{22,k} - \Delta p_{33,k}\right)^2 + \\ \left(\Delta p_{33,k} - \Delta p_{11,k}\right)^2 + 1.5\left(\Delta p_{12,k}^2 + \Delta p_{23,k}^2 + \Delta p_{31,k}^2\right)\end{array}\right]^{0.5} \tag{8}$$

Though computationally demanding, this method has the advantage of evaluating plastic strains accurately even with significant net-section plasticity and is effective for many low-cycle fatigue problems with simple load time histories. This method is currently attractive for evaluating low-cycle fatigue for loading time histories that do not have much variation. The attractiveness of Method B will gain popularity as computing capabilities evolve. For simple loading time histories the Twice Yield Method based on Massing's hypothesis may be used in lieu of a cycle-by-cycle analysis.

The effect of the weldment may be accounted for by introducing a fatigue strength reduction factor, K_f, into the strain range calculation or using the effective notch approach discussed in paragraph 2.2.1.

2.3.2. Resistance

The fatigue curve used to determine the permissible number of cycles is the same as for Method A (see Figure 5).

2.4. Level 2 Method C – Equivalent Structural Stress Range and Master S-N Curve

The technical basis and methodology for Level 2, Method C is provided in references [8-9]. The methodology was developed by Dr. Pingsha Dong, now of the University of Michigan, in studies supported by the Pressure Vessel Research Council (PVRC) of the Welding Research Council (WRC), and was found to be appropriate for standardization. The technical basis and methodology of using a Master S-N fatigue curve to characterize the behavior of welded pressure components were accepted by API and ASME, and have been incorporated into API 579-1/ASME FFS-1 and the ASME B&PV Code, Section VIII, Division 2. The Master S-N Curve Method offers not only a sound basis for design of welded components but also for remaining life assessment of welded in-service components. The major findings of the development work include the following:

- The mesh-insensitive structural stress method provides a simple and effective means for characterizing stress concentrations at pressure vessel and pipe welds.
- The structural stress-based parameter provides an effective measure of stress intensity at welds, which can be related to fatigue lives in the form of an equivalent structural stress parameter.
- With the equivalent structural stress parameter, a large amount of weld S-N data can be consolidated into one narrow scatter band. A single Master S-N curve for welds in pressure vessels and piping was proposed based on a comprehensive database of fatigue test results including studies dating back decades.
- The method is general, and it has been shown that it can be used with cumulative damage theories. Statistical analysis and the associated parameters have been used to establish the design fatigue curves. As a result, structural reliability methods (i.e., probabilistic analysis) can also be used in the design and life assessment processes.

The addition of welded joint fatigue technology to API 579-1/ASME FFS-1 and the ASME B&PV Code, Section VIII, Division 2 represented a significant departure from the legacy ASME Code methods; however, it also resulted in a significant upgrade to the evaluation methods for welded joints more in line with other international codes and standards.

2.4.1. Driving Force

2.4.1.1. Driving Force based on normal stress

The driving force is the Equivalent Structural Stress Range given by Equation (9).

$$\Delta S_{ess,k} = \frac{\Delta \sigma_k}{t_{ess}^{\left(\frac{2-m_{ss}}{2m_{ss}}\right)} \cdot I^{\frac{1}{m_{ss}}} \cdot f_{M,k}} \tag{9}$$

$$m_{ss} = 3.6 \tag{10}$$

$$I^{\frac{1}{m_{ss}}} = \frac{1.23 - 0.364 R_{b,k} - 0.17 R_{b,k}^2}{1.007 - 0.306 R_{b,k} - 0.178 R_{b,k}^2} \tag{11}$$

$$R_{b,k} = \frac{\left|\Delta \sigma_{b,k}^e\right|}{\left|\Delta \sigma_{m,k}^e\right| + \left|\Delta \sigma_{b,k}^e\right|} \tag{12}$$

$$\Delta \sigma_{m,k}^e = {}^m\sigma_{m,k}^e - {}^n\sigma_{m,k}^e \tag{13}$$

$$\Delta \sigma_{b,k}^e = {}^m\sigma_{b,k}^e - {}^n\sigma_{b,k}^e \tag{14}$$

The corresponding local nonlinear structural stress and strain ranges, $\Delta\sigma_k$ and $\Delta\varepsilon_k$, respectively, are determined by simultaneously solving Neuber's Rule, Equation (16), and a model for the material hysteresis loop stress-strain curve given by Equation (18), see API 579-1/ASME FFS-1 Part 3, Annex 3.D, paragraph 3.D.4.

$$\Delta \sigma_k^e = \Delta \sigma_{m,k}^e + \Delta \sigma_{b,k}^e \tag{15}$$

$$\Delta \sigma_k \cdot \Delta \varepsilon_k = \Delta \sigma_k^e \cdot \Delta \varepsilon_k^e \tag{16}$$

$$\Delta \varepsilon_k^e = \frac{\Delta \sigma_k^e}{E_{ya,k}} \tag{17}$$

$$\Delta \varepsilon_k = \frac{\Delta \sigma_k}{E_{ya,k}} + 2\left(\frac{\Delta \sigma_k}{2K_{css}}\right)^{\frac{1}{n_{css}}} \tag{18}$$

The thickness correction term, t_{ess}, to the Equivalent Structural Stress calculation is summarized below.

$$t_{ess} = 16 \ mm \ (0.625 \ in.) \qquad for \qquad t \leq 16 \ mm \ (0.625 \ in.) \tag{19}$$

$$t_{ess} = t \qquad for \qquad 16 \ mm \ (0.625 \ in.) < t < 150 \ mm \ (6 \ in.) \tag{20}$$

$$t_{ess} = 150 \ mm \ (6 \ in.) \qquad for \qquad t \geq 150 \ mm \ (6 \ in.) \tag{21}$$

A mean stress correction is also applied based on Equations (22) and (24).

$$f_{M,k} = 1.0 \qquad \text{for} \qquad \begin{vmatrix} \sigma_{mean,k} < 0.5 S_{y,k}, \text{ or} \\ R_k \leq 0, \text{ or} \\ \left| \Delta \sigma_{m,k}^e + \Delta \sigma_{b,k}^e \right| > 2 S_{y,k} \end{vmatrix} \qquad (22)$$

$$f_{M,k} = \left(1 - R_k\right)^{\frac{1}{m_{ss}}} \qquad \text{for} \qquad \begin{vmatrix} \sigma_{mean,k} \geq 0.5 S_{y,k}, \text{ and} \\ R_k > 0, \text{ and} \\ \left| \Delta \sigma_{m,k}^e + \Delta \sigma_{b,k}^e \right| \leq 2 S_{y,k} \end{vmatrix} \qquad (23)$$

$$R_k = \frac{\sigma_{min,k}}{\sigma_{max,k}} \qquad (24)$$

$$\sigma_{max,k} = \max \left[\left({}^m\sigma_{m,k}^e + {}^m\sigma_{b,k}^e \right), \left({}^n\sigma_{m,k}^e + {}^n\sigma_{b,k}^e \right) \right] \qquad (25)$$

$$\sigma_{min,k} = \min \left[\left({}^m\sigma_{m,k}^e + {}^m\sigma_{b,k}^e \right), \left({}^n\sigma_{m,k}^e + {}^n\sigma_{b,k}^e \right) \right] \qquad (26)$$

$$\sigma_{mean,k} = \frac{\sigma_{max,k} + \sigma_{min,k}}{2} \qquad (27)$$

2.4.1.2. Consideration of shear stress range

If the structural shear stress range is not negligible, i.e. $\Delta \tau_k > \Delta \sigma_k / 3$, a modification should be made when computing the equivalent structural stress range. Two conditions need to be considered (details are provided in [10]).

- If $\Delta \sigma_k$ and $\Delta \tau_k$ are out of phase, the equivalent structural stress range $\Delta S_{ess,k}$ in Equation (9) should be replaced by:

$$\Delta S_{ess,k} = \frac{1}{F(\delta)} \left[\left(\frac{\Delta \sigma_k}{t_{ess}^{\left(\frac{2-m_{ss}}{2m_{ss}}\right)} \cdot I^{\frac{1}{m_{ss}}} \cdot f_{M,k}} \right)^2 + 3 \left(\frac{\Delta \tau_k}{t_{ess}^{\left(\frac{2-m_{ss}}{2m_{ss}}\right)} \cdot I_\tau^{\frac{1}{m_{ss}}}} \right)^2 \right]^{0.5} \qquad (28)$$

Where

$$I_\tau^{\frac{1}{m_{ss}}} = \frac{1.23 - 0.364 R_{b\tau,k} - 0.17 R_{b\tau,k}^2}{1.007 - 0.306 R_{b\tau,k} - 0.178 R_{b\tau,k}^2} \qquad (29)$$

$$R_{b\tau,k} = \frac{\left| \Delta \tau_{b,k}^e \right|}{\left| \Delta \tau_{m,k}^e \right| + \left| \Delta \tau_{b,k}^e \right|} \qquad (30)$$

$$\Delta \tau_k^e = \Delta \tau_{m,k}^e + \Delta \tau_{b,k}^e \qquad (31)$$

$$\Delta\tau_{m,k}^e = {}^m\tau_{m,k}^e - {}^n\tau_{m,k}^e \qquad (32)$$

$$\Delta\tau_{b,k}^e = {}^m\tau_{b,k}^e - {}^n\tau_{b,k}^e \qquad (33)$$

In Equation (28), $F(\delta)$ is a function of the out-of-phase angle between $\Delta\sigma_k$ and $\Delta\tau_k$ if both loading modes can be described by sinusoidal functions, or:

$$F(\delta) = \frac{1}{\sqrt{2}}\left[1 + \left[1 - \frac{12 \cdot \Delta\sigma_k^2 \cdot \Delta\tau_k^2 \cdot \sin^2[\delta]}{\left[\Delta\sigma_k^2 + 3\Delta\tau_k^2\right]^2}\right]^{0.5}\right]^{0.5} \qquad (34)$$

A conservative approach is to ignore the out-of-phase angle and recognize the existence of a minimum possible value for $F(\delta)$ in Equation (34) given by:

$$F(\delta) = \frac{1}{\sqrt{2}} \qquad (35)$$

- If $\Delta\sigma_k$ and $\Delta\tau_k$ are in-phase the equivalent structural stress range $\Delta S_{ess,k}$ is given by Equation (28) with $F(\delta) = 1.0$.

2.4.1.3. Consideration of weld quality

If a defect exists at the toe of a weld that can be characterized as a crack-like flaw, i.e. undercut, then a reduction in fatigue life may be calculated by substituting the value of $I^{1/m_{ss}}$ in Equation (9) or Equation (28), as applicable, with the value given by Equation (36). In this equation, a is the depth of the crack-like flaw at the weld toe. Equation (36) is valid only when $a/t \le 0.1$.

$$I^{\frac{1}{m_{ss}}} = \frac{1.229 - 0.365R_{b,k} + 0.789\left(\dfrac{a}{t}\right) - 0.17R_{b,k}^2 + 13.771\left(\dfrac{a}{t}\right)^2 + 1.243R_{b,k}\left(\dfrac{a}{t}\right)}{1 - 0.302R_{b,k} + 7.115\left(\dfrac{a}{t}\right) - 0.178R_{b,k}^2 + 12.903\left(\dfrac{a}{t}\right)^2 - 4.091R_{b,k}\left(\dfrac{a}{t}\right)} \qquad (36)$$

2.4.2. Resistance

2.4.2.1. Master Fatigue Curve

The resistance to fatigue is the Master Fatigue curve given by Equation (37). The number of allowable design cycles, N, can be computed from this equation based on the equivalent structural stress range parameter, ΔS_{range}, determined above. The constants C and h for use in Equation (37) are provided in Table 5. The lower 99% Prediction Interval (-3σ) shall be used for design unless otherwise agreed to by the user and the Manufacturer.

$$N = \frac{f_I}{f_E}\left(\frac{f_{MT} \cdot C}{\Delta S_{ess,k}}\right)^{\frac{1}{h}} \qquad (37)$$

Table 5. Coefficients for the Welded Joint Fatigue Curves

Statistical Basis	Ferritic and Stainless Steels		Aluminum	
	C	h	C	h
Upper 99% Prediction Interval (+3σ)	34308.1	0.31950	6477.60	0.27712
Upper 95% Prediction Interval (+2σ)	28626.5	0.31950	5273.48	0.27712
Upper 68% Prediction Interval (+1σ)	23885.8	0.31950	4293.19	0.27712
Mean Curve	19930.2	0.31950	3495.13	0.27712
Lower 68% Prediction Interval (-1σ)	16629.7	0.31950	2845.42	0.27712
Lower 95% Prediction Interval (-2σ)	13875.7	0.31950	2316.48	0.27712
Lower 99% Prediction Interval (-3σ)	11577.9	0.31950	1885.87	0.27712

Note: In SI Units, the equivalent structural stress range parameter, $\Delta S_{ess,k}$, and the structural stress effective thickness, t_{ess}, are in $MPa/(mm)^{(2-m_{ss})/2m_{ss}}$ and mm, respectively.

2.4.2.2. Fatigue Improvement

If a fatigue improvement method is performed that exceeds the fabrication requirements of this Division, then a fatigue improvement factor, f_I, may be applied. The fatigue improvement factors shown below may be used. These factors were developed based on the work of Haagensen [11]. The inclusion of fatigue improvement methods in the fatigue analysis is considered a major step forward as these methods are known to significantly increase fatigue life and have been successfully used in many industries.

- For burr grinding

$$f_I = 1.0 + 2.5 \cdot (10)^q \tag{38}$$

- For TIG dressing

$$f_I = 1.0 + 2.5 \cdot (10)^q \tag{39}$$

- For hammer peening

$$f_I = 1.0 + 4.0 \cdot (10)^q \tag{40}$$

In the above equations, the parameter q is given by Equation (41) where the conversion factor, $C_{us} = 1$ for units of ksi.

$$q = -0.0016 \cdot \left(\frac{\Delta S_{range}}{C_{usm}} \right)^{1.6} \tag{41}$$

Note that in Equations (38) through (40), the amount of fatigue improvement is a function of the applied stress range. As shown by Haagensen [11], a greater amount of fatigue improvement is permitted as the stress range is smaller, i.e. a greater amount of fatigue improvement is obtained in the high cycle regime.

The design fatigue cycles given by Equation (37) may be modified to account for the effects of environment other than ambient air that may cause corrosion or sub-critical crack propagation. The environmental modification factor, f_E, is typically a function of the fluid environment, loading frequency, temperature, and material variables such as grain size and chemical composition. It is stipulated that a value of $f_E = 4.0$ shall be used unless there is

specific information to justify an alternate value based on the severity of the material/environmental interaction. The environmental modification factor, f_E, is required to be set by the user.

A temperature adjustment is required to the fatigue curve for materials other than carbon steel and/or for temperatures above 21°C (70°F). The temperature adjustment factor is given by Equation (42).

$$f_{MT} = \frac{E_T}{E_{ACS}}$$
(42)

The welded joint design fatigue curves in VIII-2 can be used to evaluate welded joints for the following materials and associated temperature limits:

- Carbon, Low Alloy, Series 4xx, and High Tensile Strength Steels for temperatures not exceeding 371°C (700°F)
- Series 3xx High Alloy Steels, Nickel-Chromium-Iron Alloy, Nickel-Iron-Chromium Alloy, and Nickel-Copper Alloy for temperatures not exceeding 427°C (800°F)
- Wrought 70 Copper-Nickel for temperatures not exceeding 232°C (450°F)
- Nickel-Chromium-Molybdenum-Iron, Alloys X, G, C-4, And C-276 for temperatures not exceeding 427°C (800°F)
- Aluminum Alloys

2.5. Comparison of the Level 2 Methods

A comparison of the methods is listed in Table 6 in terms of the driving force for the fatigue damage, alternating stress range, and the resistance to fatigue damage, the fatigue curve.

Table 6. Comparison of Fatigue Analysis Methods

Methods A & B (Smooth Bar Fatigue Curves)	Method C (Welded Joint Fatigue Curves)
Driving Force – Stress Measure: • Peak stress intensity from FEA continuum model • Method A: peak elastic stress directly from analysis or derived from linearized membrane and bending stress intensity against which a FSRF, K_f, is applied • Method B: equivalent elastic stress from total strains, i.e. elastic plus plastic strains • Stress linearization can be mesh sensitive, e.g., coarse mesh or 3D geometries • Fatigue penalty factor in terms of K_e for plasticity correction • Poisson's adjustment in terms of K_v • Mean stress adjustment in fatigue curve • Multi-axial effects accounted for using stress intensity or equivalent stress • Fatigue improvement, must use K_f • Weld toe defect correction, must use K_f	**Driving Force – Stress measure:** • Membrane and bending stress normal to assumed defect orientation derived from nodal forces • Stress linearization to computed structural stress is mesh-insensitive and applicable for both 2D, 3D and shell/solid models • Neuber's method for plasticity correction • Poisson's adjustment for biaxial loading • Mean stress adjustment in term of R-ratio • Multi-axial effects considered • Fatigue improvement factor explicitly included • Weld toe defect correction available
Resistance – Design Fatigue Curve: • Mean stress adjustment included in the fatigue curve • Implicit margins applied to smooth bar mean curve (2 on stress and 20 on cycles) to cover:	**Resistance – Design fatigue curve:** • Mean stress adjustment: included in structural stress driving force formulation • Explicit margins provided to welded joint fatigue curves

Table 6. Comparison of Fatigue Analysis Methods

Methods A & B (Smooth Bar Fatigue Curves)	Method C (Welded Joint Fatigue Curves)
o Scatter o Size effects o Surface condition & Environment	o Scatter: characterized by statistical measure of a large amount of actual weld S-N air data o Size effects: included in structural stress driving force formulation o Environment (f_E): not included in fatigue data scatter, explicit factor (e.g., 4) is applied o Fatigue Improvement (f_I) • Implicit margins, contained in fatigue scatter band o Surface condition including local notch effects o Welding effects

2.6. Level 3

The Level 3 assessment determines allowable fatigue cycles for a component and loading history using a multiaxial strain-life equation with a mean stress correction in combination with a critical plane approach. The critical plane approach resolves the stress-strain state at a given point on a number of candidate planes. Fatigue damage is calculated on each candidate plane using the strain-life equation, and the plane with the maximum damage identifies the critical plane and the overall fatigue damage for the given point. If an elastic-plastic analysis is performed using Level 2 Method B, strain results are post-processed directly. However, implementation of strain-life methods that use an elastic analysis are corrected for cyclic plasticity using a multiaxial Neuber correction based on a cyclic stress strain curve.

2.6.1. Driving Force

The Brown-Miller strain-life equation, adjusted for mean stress effects, shown below is used in the assessment [12]. The driving force is the applied shear strain range, $\Delta\gamma_k/2$, and normal strain range, $\Delta\varepsilon_{N,k}/2$, i.e. the LHS of Equation (43).

$$\frac{\Delta\gamma_k}{2} + \frac{\Delta\varepsilon_{N,k}}{2} = 1.65 \cdot \frac{\left(\sigma'_{f,k} - \sigma_{N-mean,k}\right)}{E_{ya,k}} \cdot \left(2N_{f,k}\right)^{b_k} + 1.5\varepsilon'_{f,k}\left(2N_{f,k}\right)^{c_k} \tag{43}$$

Plasticity correction is accounted for using an incremental Neuber procedure suitable for non-proportional loading [2, 12-13]. The plasticity model incorporated is the multiple backstress, nonlinear kinematic-hardening model of Chaboche [14-15]. Strain results are post-processed directly if an elastic-plastic analysis is performed. A multi-channel rainflow procedure has also been developed to identify cycles on the critical planes, see reference [2]. The effect of the weldment may be accounted for by using the effective notch approach discussed in paragraph 2.2.1.

2.6.2. Resistance

The resistance is the RHS of Equation (43) and is characterized by the parameters, $\sigma'_{f,k}$, b_k, $\varepsilon'_{f,k}$ and c_k. The fatigue curve parameters and cyclic stress-strain curve may be derived from the Uniform material Law [16].

3. Ratcheting

3.1. Definition

Ratcheting is a progressive incremental inelastic deformation or strain that can occur in a component subjected to variations of mechanical stress, thermal stress, or both (thermal stress ratcheting is partly or wholly caused by mechanical stress). Ratcheting is produced by a sustained load acting over the full cross section of a component, in combination with a strain controlled cyclic load or temperature distribution that is alternately applied and removed. Ratcheting causes cyclic straining of the material, which can result in failure by fatigue and at the same time produces cyclic incremental growth of a structure, which could ultimately lead to collapse (see Figure 6).
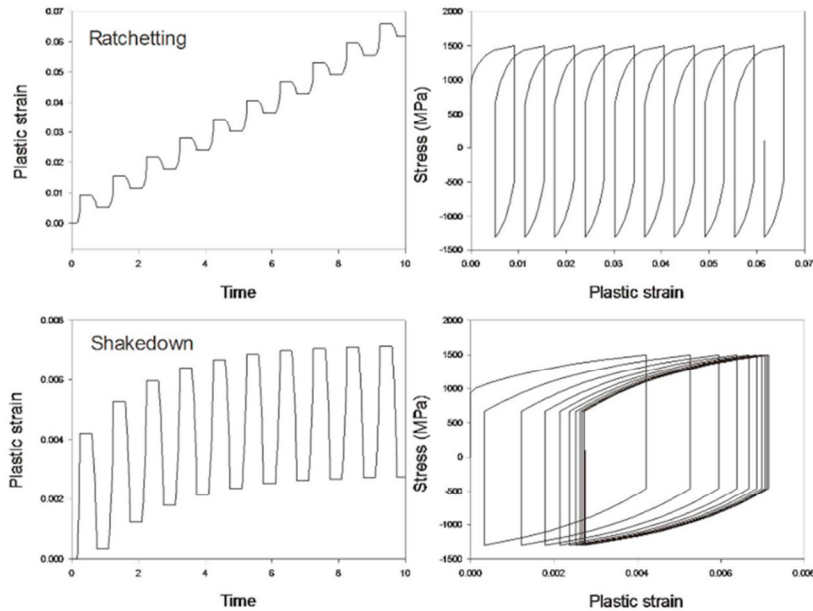
Figure 6. Ratcheting and shakedown (courtesy of the ANSYS Blogg)

The ASME B&PV Code, Section VIII, Division 2 provides rules to preclude ratcheting in design by using the results of an elastic stress analysis with the Bree Diagram. This design methodology ensures that shakedown to elastic action for membrane plus bending stresses will occur on any section through the wall of a pressurized component. In addition, membrane plus bending plus peak stresses on the same section will result in a stabilized hysteresis loop.

3.2. Bree Diagram

In the 1950's, Weil and Rapasky [17] and Coffin [18-19] observed that thin-walled pressure vessels subjected to a constant axial stress and a cyclic thermal stress demonstrated progressive distortion. To better understand this behavior, Miller [20-21] conducted an analytical investigation of a pressure vessel subjected to a through-wall cyclic thermal gradient. He assumed an elastic-perfectly plastic material model with a constant and uniform axial stress. Miller first used a simplified three-bar assembly to illustrate that, if the thermal strains and the tensile membrane stress due to pressure are sufficiently high, an increment of inelastic strain (growth) will be produced by each thermal cycle. This increment of growth is known as inelastic ratcheting. Then, Miller extended his investigation to consider the case of a thin-walled cylinder with an internal pressure and a cyclic thermal stress. Similar to his conclusions from the three-bar assembly, he found that under sufficiently high loads the cylinder will be subject to incremental growth.

Approximately a decade later, in the late 1960's, Bree [22] formalized the work of Miller and created a diagram that has become a staple in many codes and standards today including API 579-1/ASME FFS-1 and the ASME B&PV Code, Section VIII, Division 2. The Bree diagram plots the primary membrane stress versus the cyclic thermal stress and delineates the various zones of plastic behavior; namely

- E – elastic cycling
- P1, P2, P3 – plastic cycling
- S1 – elastic cycling after initial one-sided plasticity (i.e. "shakedown"),
- S2 – elastic cycling after initial two-sided plasticity (i.e. "shakedown"), and
- R1 – ratcheting, one-sided yielding
- R2 – ratcheting, two sided yielding

The original Bree diagram is reproduced here in Figure 7 with $R = 1.0$ where $R = \sigma_{y-hot} / \sigma_{y-cold}$. Bree also derived analytical expressions for the increment of plastic strain per cycle when ratcheting occurs.

The simplicity of the Bree diagram has led to its widespread adoption by practitioners, however, this has also led to its misapplication for problems outside the boundaries for which it was initially intended. The primary assumptions used in the development of the original Bree diagram include:

- The primary membrane stress is held constant while the secondary thermal stress is cycled,
- The yield stress is independent of temperature,
- There are no creep induced inelastic strains, and
- The material behavior is elastic-perfectly plastic.

While these assumptions made it possible to obtain analytical expressions delineating the various zones of straining behavior, they do not adequately represent realistic materials. Actual materials have temperature dependent properties and display creep strains under sustained loads. The yield stress of some steels commonly used in pressure vessels can vary by a factor of two during startup and shutdown events. Moreover, under high thermal loads, both plastic strains and creep strains contribute to the magnitude of incremental growth during ratcheting. Thus, the inclusion of high temperature creep effects in the analysis alter the range of operating conditions that lead to ratcheting.

In 1981, Moreton and Ng modified the original Bree diagram to account for cases with in-phase and out-of-phase cycling of the primary and thermal stresses [23]. These diagrams have been widely incorporated into various codes and standards. However, shortly after publication, Moreton and Ng published a series of papers correcting some oversight made in their original derivation–expanding the diagrams for greater precision in the plastic behavior [24-26]. These papers correcting the original, 1981, diagrams went largely unnoticed. As commonly occurs in the scientific community, these revised diagrams have recently been independently re-derived and republished [27].

3.3. Bree Diagram assumptions

The Bree problem considers a thin-walled cylinder of width t, subjected to a primary membrane stress, σ_m, and a secondary thermal stress, σ_t [22-28]. To simplify the analysis, it is assumed that the radius of the cylinder is much less than its length and that the wall thickness is much less than the radius. Thus, the effects of curvature can be neglected and, if it is assumed that the axial stress is negligible, the problem can be approximated with a uniaxial model in the hoop direction [22]. Additionally, the primary membrane (hoop) stress is assumed to be a result of an internally applied pressure and is held constant, while the secondary thermal stress cycles between 0 and σ_t, as illustrated in Figure 7. The secondary thermal stress is strain controlled and the wall of the cylinder is assumed to be fully restrained against bending. With these boundary conditions, a net membrane strain arises and the total bending strain is zero.

3.4. Code implementation

The Bree diagram represents a conservative design tool for the prevention of ratcheting using the results from an elastic stress analysis. It should be noted that the assumptions of the Bree Diagram are consistent with the stress categorization methodology represented by the Hopper Diagram (see Figure 2). Spring [29] has re-derived the Bree diagram for four loading cases including a change in the yield strength between the cold and hot portions of the cycle. In each of these cases the material behavior is assumed to be elastic-perfectly plastic. The four case are defined as follows:

- Cyclic Load Type A – Constant primary membrane stress, σ_p, and cyclic secondary bending stress, σ_{ss} (see Table 7 and Figure 7).
- Cyclic Load Type B – Cyclic primary membrane stress, σ_p, and cyclic secondary bending stress, σ_{ss}, that are in-phase (see Table 8 and Figure 8).
- Cyclic Load Type C – Cyclic primary membrane stress, σ_p, and cyclic secondary bending stress, σ_{ss}, that are out-of-phase (see Table 9 and Figure 9).
- Cyclic Load Type D – Cyclic primary membrane stress, σ_p, and constant secondary bending stress, σ_{ss} (see Table 10 and Figure 10).

The full derivation of each load type will be published in a forthcoming Welding Research Council Bulletin [30]. Currently only Cyclic Load Type A is included in API 579-1/ASME FFS-1 and the ASME B&PV Code, Section VIII, Division 2 where the effects of the change in the yield stress from hot to cold is smeared by using the average value between the two temperature extremes of the cycle. However, in future releases of both codes it has been recommended to include all four case with the effects of the change in yield strength between the cold and hot portions of the cycle.
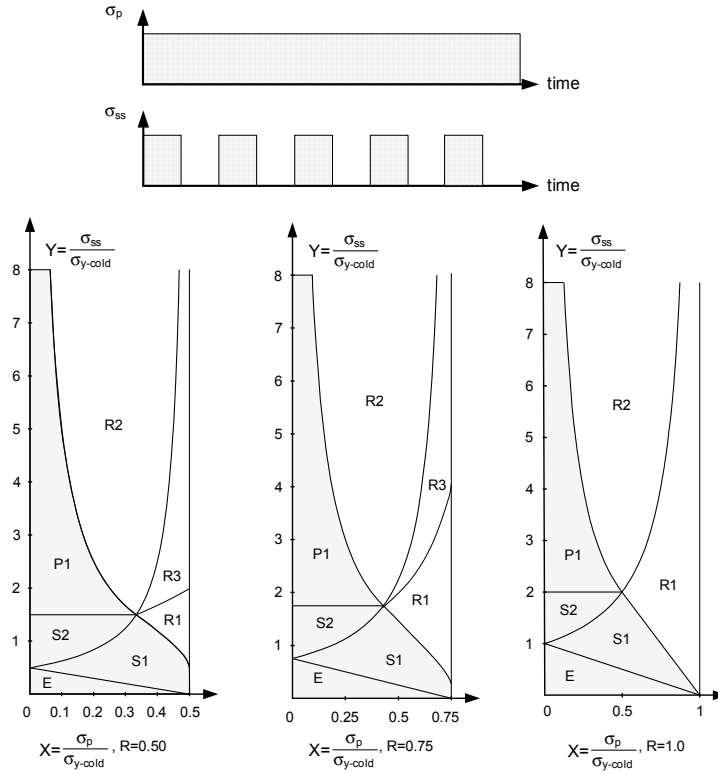
Figure 7. Cyclic Load Type A: Regions and Boundaries for the Bree Diagram (R = 0.50, 0.75 and 1.0)

Table 7. Expressions for Delimiting the Bree diagram in Figure 7.

Region	Boundaries	Ratchet Strain ($E\varepsilon_R / \sigma_{y-cold}$)
E	*Below*: $X + Y = R$	---
S1	*Above*: $X + Y = R$ *Below*: $Y(R - X) = R^2$ *Below*: $Y = \left(\sqrt{R - X} + \sqrt{1 - X}\right)^2$	---
S2	*Above*: $Y(R - X) = R^2$ *Below*: $Y = R + 1$	---
P1	*Above*: $Y = R + 1$ *Below*: $XY = R$	---
R1	*Above*: $Y = \left(\sqrt{R - X} + \sqrt{1 - X}\right)^2$ *Below*: $Y(R - X) = R^2$	$2Y - 2\sqrt{Y(R - X)} - 2\sqrt{Y(1 - X)}$
R2	*Above*: $Y(R - X) = R^2$ *Above*: $XY = R$	$\dfrac{XY}{R} + XY - R - 1$
R3	*Above*: $Y(1 - X) = 1$ *Below*: $Y(R - X) = R^2$	$XY - 1 - Y + 2\sqrt{Y(R - X)}$
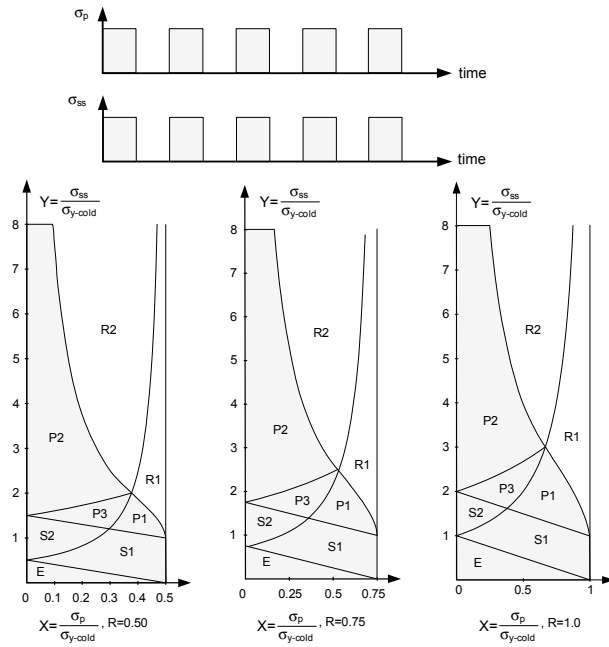
Figure 8. Cyclic Load Type B: Regions and Boundaries for the Bree Diagram with In-Phase Cyclic Primary Stress and Cyclic Secondary Stress (R = 0.50, 0.75 and 1.0)

Table 8. Expressions for Delimiting the Bree diagram in Figure 8.

Region	Boundaries	Ratchet Strain ($E\varepsilon_R / \sigma_{y-cold}$)
E	$Below: X + Y = R$	---
S1	$Above: X + Y = R$ $Below: Y(R - X) = R^2$ $Below: X + Y = 1 + R$	---
S2	$Above: Y(R - X) = R^2$ $Below: X + Y = 1 + R$	---
P1	$Above: X + Y = 1 + R$ $Below: Y(R - X) = R^2$ $Below: 0.25(2 + 4R - Y - Y^{-1}) = X$	---
P2	$Above: Y(1 + R - X) = (1 + R)^2$ $Below: XY = R(1 + R)$	---
P3	$Above: X + Y = 1 + R$ $Above: Y(R - X) = R^2$ $Below: Y(1 + R - X) = (1 + R)^2$	---
R1	$Above: 0.25(2 + 4R - Y - Y^{-1}) = X$ $Below: Y(R - X) = R^2$	$Y - 1 - 2\sqrt{Y(R - X)}$
R2	$Above: Y(R - X) = R^2$ $Above: XY = R(1 + R)$	$\dfrac{XY}{R} - R - 1$
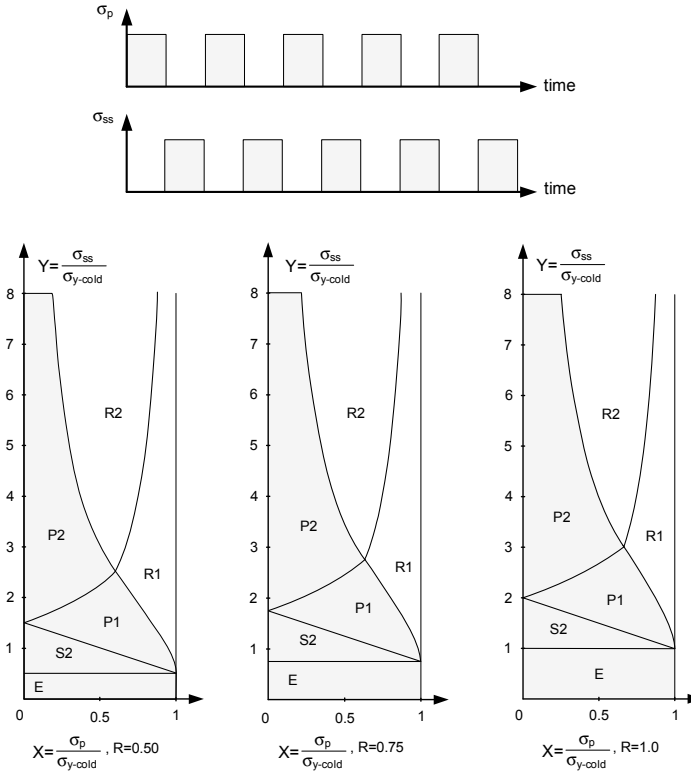
Figure 9. Cyclic Load Type C: Regions and Boundaries for the Bree Diagram with Out-Of-Phase Cyclic Primary Stress and Cyclic Secondary Stress (R = 0.50, 0.75 and 1.0)

Table 9. Expressions for Delimiting the Bree diagram in Figure 9.

Region	Boundaries	Ratchet Strain ($E\varepsilon_R / \sigma_{y-cold}$)
E	*Below*: $Y = R$	---
S2	*Above*: $Y = R$ *Below*: $X + Y = 1 + R$	---
P1	*Above*: $X + Y = R + 1$ *Below*: $Y(1 + R - X) = (1 + R)^2$ *Below*: $0.25(4 + 2R - Y - R^2 Y^{-1}) = X$	---
P2	*Above*: $Y(1 + R - X) = (1 + R)^2$ *Below*: $XY = 1 + R$	---
R1	*Above*: $0.25(4 + 2R - Y - R^2 Y^{-1}) = X$ *Below*: $Y(1 - X) = 1$	$Y - R - 2\sqrt{Y(1 - X)}$
R2	*Above*: $Y(1 - X) = 1$ *Above*: $XY = 1 + R$	$XY - R - 1$
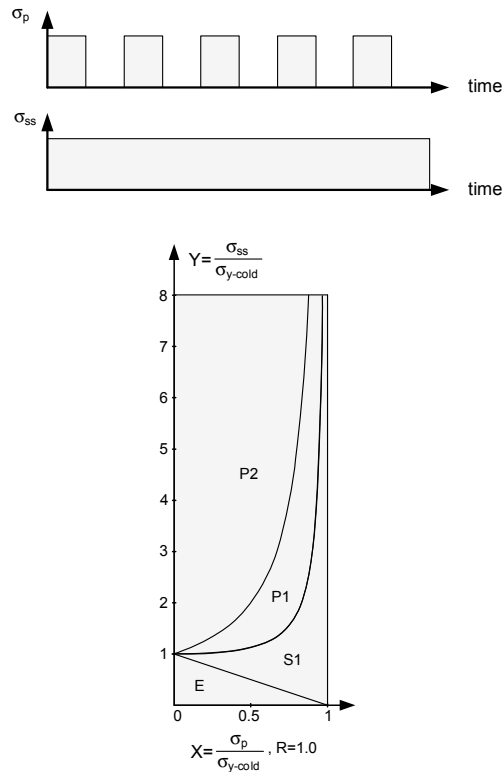
Figure 10. Cyclic Load Type D: Regions and Boundaries for the Bree Diagram with a Cyclic Primary Stress and a Constant Secondary Stress (R= 1.0)

Table 10. Expressions for Delimiting the Bree diagram in Figure 10.

Region	Boundaries	Ratchet Strain ($E\varepsilon_R / \sigma_{y-cold}$)
E	*Below*: $X + Y = 1$	---
S1	*Above*: $X + Y = 1$ *Below*: $\sqrt{Y(1-X)} + 0.5X = 1$	---
P1	*Above*: $\sqrt{Y(1-X)} + 0.5X = 1$ *Below*: $Y(1-X) = 1$	---
P2	*Above*: $Y(1-X) = 1$	---

4. Fatigue Assessment of Welds Using the Equivalent Structural Strain Method

4.1. Overview

   The Master S-N curve described in paragraph 2.4 was developed by introducing an equivalent structural stress range parameter that collapses a large number of fatigue test data (i.e. approximately 1000 tests of large scale and full scale specimens) into a narrow scatter band. These tests span a wide range of joint geometries, plate or pipe wall thicknesses, and loading modes. The test data on which the Master S-N curve was based have fatigue lives with a range of a few hundred cycles to as long as nearly 10^8 cycles to failure. It should be noted that in the low

cycle regime, i.e., typically lower than 10^4 or 10^5, pseudo-elastic structural stress ranges [9,31] are based on reported pseudo-elastic loads in displacement controlled low-cycle fatigue tests, such as those in [32-33].

In supporting the development of a welded joint fatigue method for API 579-1/ASME FFS-1 and the ASME B&PV Code, Section VIII, Division 2, Dong et al [31] proposed a preliminary low-cycle fatigue (LCF) treatment procedure for adapting the master S-N curve method which was mainly focused upon high-cycle fatigue to low-cycle fatigue applications in pressure vessels mostly subjected to load-controlled conditions. The procedure involves converting elastically calculated structural stresses under a given loading condition into a through-thickness linearly distributed structural strain according to Hooke's law, then searching for a structural strain definition that satisfies both yield conditions and through-thickness linear deformation conditions. At the time it was assumed that Neuber's rule could be used to calculate approximate structural strains beyond yield using the elastically calculated structural stresses. The resulting structural strain parameter is then used to obtain pseudo-elastic structural stresses by applying Hooke's law or multiplying Young's modulus if assuming a uniaxial stress state prevails (see Equations (16) through (18)). Although showing an improved fatigue life estimation over a purely elastic-based assessment procedure (i.e., without any plastic deformation considerations) for limited available low-cycle fatigue test data [34], there exist a number of inconsistencies or weaknesses in that approach as outlined below.

- Although a structural strain concept was first introduced in [35], its implementation in the elastic-plastic deformation regime was largely incomplete in view of the fact that a local strain definition had to be used to approximate structural strain according Neuber's rule which has typically been used for notch stress and strain characterization beyond the elastic regime. As a result, the very structural strain definition intended to characterize linear through-thickness deformation no longer possesses its original meaning.
- It is preferable that any low cycle fatigue correction procedure should provide an indication on the extent of plastic deformation, e.g., elastic core size. The presence of an elastic core is important since it helps justify an approximate proportionality in fatigue damage accumulation so that an elastic finite element stress analysis can still be used in fatigue design. To the authors' best knowledge, existing low-cycle fatigue procedures [31, 33, 36-37] for welded structures are not capable of providing any information regarding whether an elastic core is still present, nor its size at a location of interest.
- Lastly, one advantage of the nodal force based structural stress definition is its statically equivalent decomposition of a through-thickness traction stress state in terms of membrane and bending. Once Neuber's rule is applied for estimating structural strains in elastic-plastic deformation regime, the previous method [31] is no longer capable of tracking membrane and bending composition or bending ratio after calculating the pseudo elastic structural stress. As a result, elastic bending ratio must be used to calculate the equivalent pseudo-elastic structural stress range in order to use the design master S-N curve. Fortunately, under strictly load controlled conditions, fatigue lives are only weakly dependent upon bending ratio [9]. However under-displacement controlled conditions, a much stronger dependency has been shown in [9]. Therefore, an improved treatment of low-cycle fatigue is needed.

A structural strain procedure has been developed [4] that is consistent both with the mesh-insensitive structural stress method [8-9] and the original intent expressed in [31] when the terminology of structural strain was perhaps first introduced for the treatment of low cycle fatigue. In the following paragraphs, a structural strain definition valid for both elastic and elastic-plastic deformation regimes is then presented. Analytical solutions of structural strains and the resulting elastic core size are then presented by assuming elastic perfectly-plastic material response. Finally, modification of the exiting Level 2, Method C method in paragraph 2.4 to incorporate the structural strain approach is provided.

4.2. Structural Strain Method

Consistent with classical plate theory, a structural member going through elastic or elastic-plastic deformation is assumed to deform in such a way that a through-thickness plane normal to the plate mid-surface before deformation remains plane after deformation. For simplicity, but without losing generality, the material response can be further assumed to be isotropic and elastic perfectly plastic. Additionally, it is assumed that only the normal traction stress

is operative. Two cases are considered here: one is bending-dominated loading that may generate plastic deformation at both plate surfaces; the other is membrane-dominated loading that may develop plastic deformation at one plate surface.

4.2.1. Bending-dominated loading – two-sided yielding of the cross section

For a through-thickness hypothetical cut, an elastically calculated normal traction stress is depicted as σ_m and σ_b in Figure 11.
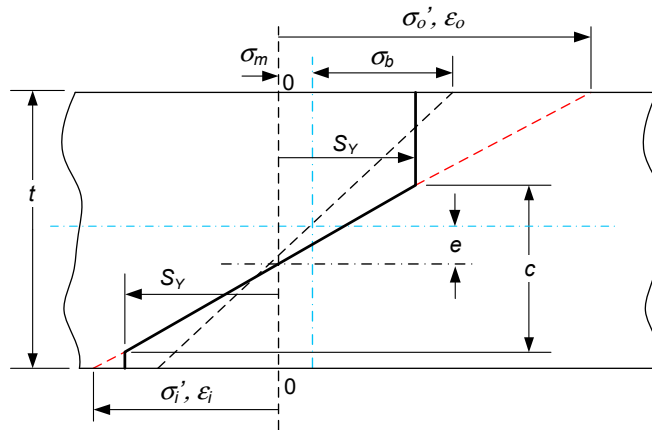
Figure 11. Schematic of the structural strain parameters for the two-sided yield condition.

The combined normal traction stress in this case exceeds the material yield strength S_Y. Therefore, the linear-elastically calculated normal traction stress distribution in terms of σ_m and σ_b must be re-distributed to satisfy equilibrium conditions (i.e., force and moment balances) and yield criterion (here it is assumed von Mises criterion is applicable). The resulting stress distribution (see Appendix for derivation details) is shown as the thick lines in Figure 11. Parameters c and e represent the corresponding elastic core size and shift of the neutral axis of bending, respectively,

$$c = t \sqrt{3 \left[1 - \left(\frac{\sigma_m}{S_Y} \right)^2 - \frac{2\sigma_b}{3S_Y} \right]} \qquad (44)$$

$$e = \frac{\sigma_m t}{2 S_Y} \qquad (45)$$

Equation (44) yields the well-known classical limit stress state of $\sigma_b = 3S_Y / 2$ if $\sigma_m = 0$ and $c = 0$. A non-zero elastic core condition can be stated as (for a two-sided yield condition):

$$\frac{c}{2} < \frac{t}{2} - e \qquad (46)$$

Assuming the presence of an elastic core dominates the through-thickness deformation behavior, one can show the resulting curvature of bending becomes:

$$\frac{1}{R} = \frac{2S_Y}{cE} \qquad (47)$$

where R represents the bending radius or radius of curvature. Then, the structural strains at both outer and inner fibers become:

$$\varepsilon_o = \frac{1}{R}\left(e + \frac{t}{2}\right) \qquad (48)$$

$$\varepsilon_i = \frac{1}{R}\left(e - \frac{t}{2}\right) \qquad (49)$$

Then, a pseudo elastic structural stresses analogous to the pseudo-elastic nominal stresses used in reference [31,34-35] in low-cycle fatigue testing can then be obtained by multiplying by the Young's Modulus of the material as:

$$\sigma_m' = \frac{E\sigma_m t}{2RS_Y} \qquad (50)$$

$$\sigma_b' = \frac{Et}{2R} \qquad (51)$$

The complete derivation of all equations for this case are provided in Paragraph A.2.

4.2.2. Membrane-dominated loading – one-sided yielding of the cross section

If σ_m is relatively high, plastic deformation may only occur near the outer surface, i.e., $\sigma_i' \le S_Y$, illustrated in Figure 12.
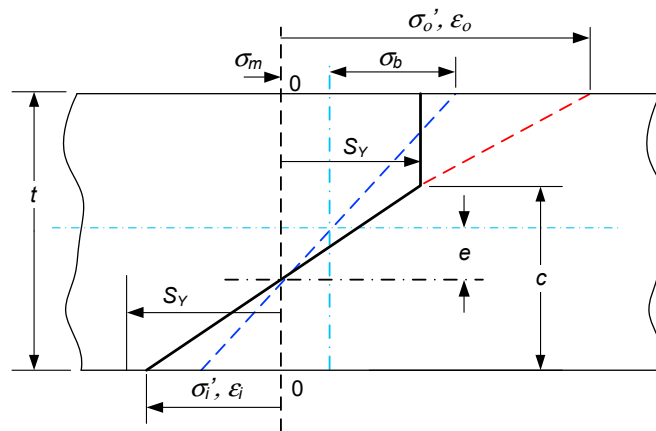
Figure 12. Schematic of the structural strain parameters for the one-sided yield condition.

By a similar derivation process to the one in Section 4.2.1, the elastic core size c can be expressed as:

$$c = \frac{t}{2}\left(\frac{3S_Y - 3\sigma_m - \sigma_b}{S_Y - \sigma_m}\right) \tag{52}$$

and the resulting curvature of bending as,

$$\frac{1}{R} = \frac{8(S_Y - \sigma_m)^3}{tE(3S_Y - 3\sigma_m - \sigma_b)^2} \tag{53}$$

Then, structural strains at both outer and inner surfaces have the following expressions:

$$\varepsilon_0 = \frac{S_Y}{E} + \frac{(t-c)}{R} \tag{54}$$

$$\varepsilon_i = \frac{S_Y}{E} - \frac{c}{R} \tag{55}$$

The pseudo-elastic structural stresses become:

$$\sigma'_m = S_Y + \frac{E}{2R}(t - 2c) \tag{56}$$

$$\sigma'_b = \frac{tE}{2R} \tag{57}$$

It is not surprising that the pseudo-elastic bending stress component σ_b' in Equation (56) has an identical expression to the one in Equation (51) since the bending stress by definition is only related to curvature $1/R$ and Young's Modulus. The complete derivation of all equations for this case are provided in Paragraph A.1.

4.2.3 Plain strain conditions and nonlinear hardening

In structural life evaluation, plane strain conditions often prevail. Treatment of plane strain conditions under elastic perfectly plastic conditions, although following the same formulation process as described in the previous section, requires a numerical solution procedure for elastic core size c (or radius of curvature, R) and neutral axis position e under a given set of σ_m, σ_b, and S_y. To simplify the calculation procedure for performing fatigue evaluation in practice, Pei et al [3] provided graphic solutions in terms of radius of curvature (R) and neutral axis position e, as shown in Figure 13. Then, the structural strain corresponding to the conditions illustrated in Figures 11 and 12 can be written as

$$\varepsilon_o = \frac{y - e}{R + e} \tag{58}$$

Note that with the aid of Figure 13, differentiation between one-sided yielding (Figure 12) and two-sided yielding (Figure 11) is no longer necessary since this consideration has already been taken into account during the construction of Figure 13, which further simplifies the solution procedure in practice. The graphic solutions in Figure 13 can also be presented in a form of tabulated solutions or polynomial fits for convenience, if so desired.

The theory for the development of Figure 13 is given in [3], in which a unified structural strain calculation method by considering Ramberg-Osgood material hardening behavior is also presented, as a part of WRC/PVRC

Joint Industry Project (JIP) project on enhanced fatigue evaluation procedures that is currently on going [38]. An analytical structural strain calculation procedure for pipe section is also given in Pei et al [39], which provides an efficient calculation procedure for determining structural strain without the need of FEA.
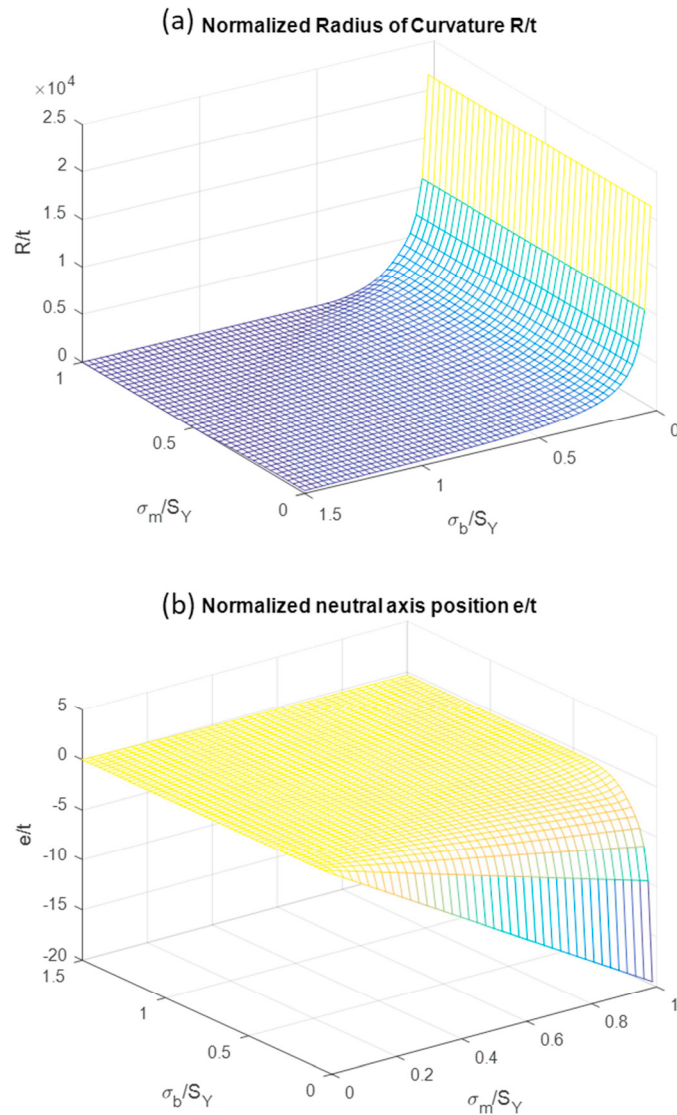
Figure 13. Normalized radius of curvature (R) and neutral axial position (e) as a function of normalized membrane and bending stresses: (a) radius of curvature (R); (b) neutral axis position (e)

4.2.3. Modification of Level 2, Method C

A step-by-step produce is used to show the implementation of the structural strain method in Level 2, Method C described in paragraph 2.4.1.1.

- Step 1 – The modification of Level 2, Method C starts with the Bree Diagrams as presented in paragraph 3.4. Based on the applied loading, select the Cyclic Load Type from paragraph 3.4.

- Step 2 – Determine the primary membrane stress, σ_p, and the secondary stress, σ_{ss}.
- Step 3 – Determine the yield stress at the coldest portion of the cycle, σ_{y-cold}, and the yield stress at the hottest portion of the cycle, σ_{y-hot}.
- Step 4 – Determine the ratio of the hot to cold yield stresses from Step 3, $R = \sigma_{y-hot} / \sigma_{y-cold}$.
- Step 5 – Determine the primary stress ratio $X = \sigma_p / \sigma_{y-cold}$ and the secondary stress ratio $Y = \sigma_{ss} / \sigma_{y-cold}$.
- Step 6 – Based on the Cyclic Load Type from Step 1, the ratio of the hot to cold yield stresses from Step 4, and the primary and secondary stress ratios from Step 5, determine the region on the Bree Diagram associated with the applied loading.
- Step 7 – The number of permissible cycles is determined as follows.
- Step 7.1 – If the region on the Bree Diagram is E, then the equivalent structural stress range is computed using the equations in paragraph 2.4.1.1; however, Equation (15) is used directly, or $\Delta\sigma_k = \Delta\sigma_k^e = \Delta\sigma_{m,k}^e + \Delta\sigma_{b,k}^e$.
- Step 7.2 – If the region on the Bree Diagram is S1, then the equivalent structural stress range is computed using the equations in paragraph 2.4.1.1; however, ${}^m\sigma_{m,k}^e$ & ${}^n\sigma_{m,k}^e$ are based on Equation (56), ${}^m\sigma_{b,k}^e$ & ${}^n\sigma_{b,k}^e$ are based on Equation (57), and Equation (15) is used directly, or $\Delta\sigma_k = \Delta\sigma_k^e = \Delta\sigma_{m,k}^e + \Delta\sigma_{b,k}^e$.
- Step 7.3 – If the region on the Bree Diagram is S2, then the equivalent structural stress range is computed using the equations in paragraph 2.4.1.1; however, ${}^m\sigma_{m,k}^e$ & ${}^n\sigma_{m,k}^e$ are based on Equation (50), ${}^m\sigma_{b,k}^e$ & ${}^n\sigma_{b,k}^e$ are based on Equation (51), and Equation (15) is used directly, or $\Delta\sigma_k = \Delta\sigma_k^e = \Delta\sigma_{m,k}^e + \Delta\sigma_{b,k}^e$.
- Step 7.4 – If the region on the Bree Diagram is P1, P2, P3, R1, R2, or R3, then shakedown will not occur. Regions P1, P2, and P3 indicate that alternating plasticity will occur under primary plus bending loading, and regions R1, R2 and R3 indicate that ratcheting will occur under primary plus bending loading. For regions R1, R2 and R3, an elastic core throughout the cycle does not exist, i.e. $c = 0$. Typically in these cases, static strength design criteria might have already predicted structural deficiencies before invoking the needs for low-cycle fatigue evaluation.

5. Summary

In this paper, an overview of the fatigue analysis methods for welded joints in API 579-1/ASME FFS-1 is provided. Fatigue methods based on smooth bar and welded joints are covered; Level 2, Method A and Method B, and Level 3. In the application of the smooth bar fatigue curves, either elastic or elastic plastic stress analysis may be used in conjunction with a fatigue strength reduction factor or the incorporation of an effective notch in the mesh may be used. Recommendations are provided for fatigue strength reduction factors; however the fatigue results may be mesh dependent. To resolve the singularity that occurs in a finite element mesh associated with the toe of a weld, a notch may be introduced; however, the size of the notch and the resulting size of the model, i.e. number of degrees of freedom, may prove limiting in the application. In the application of the welded joint fatigue curves, Level 2, Method C, only the membrane and bending stress need to be computed to determine the equivalent structural stress range, and a Neuber correction is used for primary plus secondary loading that results in low-cycle fatigue. The main benefits of this method are ease of use, i.e. shell elements may be used in the finite element analysis because only membrane and bending stresses are required, the fatigue results are mesh independent and there is no need to determine a fatigue strength reduction factor or to introduce notches into the finite element mesh.

As an enhancement of the welded joint method based on the equivalent structural stress range, a new structural strain method is presented. The structural strain method is formulated based on the basic assumption of classical plate and shell theory in which linear through-thickness deformation gradient is assumed a priori. Under the assumption of elastic and perfectly plastic materials, a set of analytical solutions of structural strain and elastic core size have been developed and validated using available test data. The method can be readily extended to materials wherein strain hardening effects need to be considered, for which numerical solution techniques can be used for obtaining final structural strain solutions.

The ratcheting assessment in API 579-1/ASME FFS-1 using the results of an elastic stress analysis is based on the Bree Diagram. The Bree diagram can used to determine elastic or shakedown conditions based on the applied cyclic loading. For elastic conditions (E), the current equivalent structural stress range is used in the analysis. For the shakedown condition (S1 & S2, i.e. one-sided and two-sided yielding), an elastic core is present and an equivalent structural stress range may be computed based on a structural strain range. A step-by-step procedure illustrating the fatigue calculation is provided.

Acknowledgements

Appendix A. Derivation of the Structural Strain Method

Here, the full derivation of the structural strain method for one-sided and two-sided yielding is presented.

A.1. One-Sided Yielding Condition

From the requirement of equilibrium of the internal stress with the external stress, the balance of forces yields, from Figure A.1:

$$\sigma_m t = (t-c)S_y + c\left(\frac{S_y + \sigma_1}{2}\right) \tag{A.59}$$
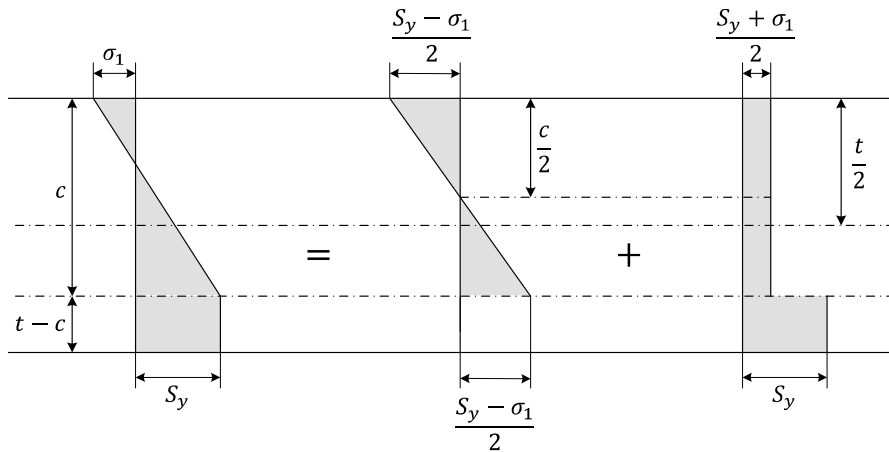
Figure A.1. Break down of one side yielding stress distribution into an antisymmetric linear distribution and two uniform elastic and plastic distributions.

Solving Equation (A.59) for σ_1 yields:

$$\sigma_1 = \frac{2\sigma_m t}{c} - \frac{2S_y t}{c} + S_y \tag{A.60}$$

Similarly, taking moments about the midline, in reference to Figure A.1, the balance of moments yields:

$$\frac{\sigma_b t^2}{6} = \frac{c^2}{6}\left(\frac{S_y - \sigma_1}{2}\right) + S_y\left(t - c\right)\left(\frac{t}{2} - \frac{1}{2}(t - c)\right) - c\left(\frac{S_y + \sigma_1}{2}\right)\left(\frac{t}{2} - \frac{c}{2}\right) \tag{A.61}$$

Simplifying and rearranging Equation (A.61) yields:

$$\frac{\sigma_b t^2}{6} = \frac{c^2 S_y}{12} - \frac{c^2 \sigma_1}{12} + S_y\left(t - c\right)\left(\frac{c}{2}\right) - \left(\frac{1}{4}\right)\left(S_y + \sigma_1\right)\left(tc - c^2\right) \tag{A.62}$$

$$\frac{\sigma_b t^2}{6} = \frac{c^2 S_y}{12} - \frac{c^2 \sigma_1}{12} + \frac{tc S_y}{2} - \frac{c^2 S_y}{2} - \frac{tc S_y}{4} + \frac{c^2 S_y}{4} - \frac{tc \sigma_1}{4} + \frac{c^2 \sigma_1}{4} \tag{A.63}$$

$$2\sigma_b t^2 = -2c^2 S_y + 2c^2 \sigma_1 + 3tc S_y - 3tc \sigma_1 \tag{A.64}$$

$$2\sigma_b t^2 = 3tc S_y - 2c^2 S_y + \left(2c^2 - 3tc\right)\sigma_1 \tag{A.65}$$

Substituting Equation (A.60) into Equation (A.65) for σ_1 yields:

$$2\sigma_b t^2 = 3tc S_y - 2c^2 S_y + \left(2c^2 - 3tc\right)\left(\frac{2\sigma_m t}{c} - \frac{2S_y t}{c} + S_y\right) \tag{A.66}$$

Simplifying and rearranging Equation (A.66) yields:

$$2\sigma_b t^2 = 3tc S_y - 2c^2 S_y + 4c\sigma_m t - 4c S_y t + 2c^2 S_y - 6\sigma_m t^2 + 6S_y t^2 - 3tc S_y \tag{A.67}$$

$$\sigma_b t^2 + 3\sigma_m t^2 - 3S_y t^2 = 2ct\left(\sigma_m - S_y\right) \tag{A.68}$$

Solving Equation (A.68) for c yields:

$$c = \frac{t}{2}\left(\frac{\sigma_b + 3\sigma_m - 3S_y}{\sigma_m - S_y}\right) = \frac{t}{2}\left(\frac{3S_y - \sigma_b - 3\sigma_m}{S_y - \sigma_m}\right) \tag{A.69}$$

In the structural strain method, the elastic core is assumed to dominate the through-thickness deformation behavior, and so the radius of curvature can be determined as the ratio of the strain in the elastic core to $c/2$, as illustrated in Figures A.2 and 12.
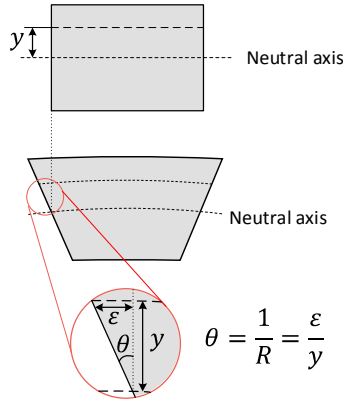
Figure A.2. Relation between the radius of curvature and the strains within a beam subjected to bending

$$\frac{1}{R} = \frac{S_y - \sigma_1}{2E}\left(\frac{1}{c/2}\right) = \frac{S_y - \sigma_1}{cE} \tag{A.70}$$

Substituting Equation (A.60) into Equation (A.70) for σ_1 yields:

$$\frac{1}{R} = \frac{S_y - \left(\dfrac{2\sigma_m t}{c} - \dfrac{2S_y t}{c} + S_y\right)}{cE} \tag{A.71}$$

Simplifying Equation (A.71) yields:

$$\frac{1}{R} = \frac{2t\left(S_y - \sigma_m\right)}{c^2 E} \tag{A.72}$$

Substituting Equation (A.69) into Equation (A.72) for c yields:

$$\frac{1}{R} = \frac{2t\left(S_y - \sigma_m\right)}{E}\left(\frac{4}{t^2}\right)\left(\frac{S_y - \sigma_m}{3S_y - \sigma_b - 3\sigma_m}\right)^2 \tag{A.73}$$

$$\frac{1}{R} = \frac{8\left(S_y - \sigma_m\right)^3}{Et\left(3S_y - \sigma_b - 3\sigma_m\right)^2} \tag{A.74}$$

Structural Strain at the outer and inner surface can be determined using linear extrapolation of the strain at the onset of yield, from Figure A.2:

$$\varepsilon_o = \frac{S_y}{E} + \frac{t - c}{R} \tag{A.75}$$

$$\varepsilon_i = \frac{S_y}{E} - \frac{c}{R} \tag{A.76}$$

From the strains at the outer and inner surface, a pseudo elastic structural membrane stress can be obtained:

$$\sigma'_m = \frac{\sigma'_o + \sigma'_i}{2} = \frac{E\varepsilon_o + E\varepsilon_i}{2} \tag{A.77}$$

Substituting Equations (A.75) and (A.76) into Equation (A.77) yields:

$$\sigma'_m = \frac{E}{2}\left(\frac{S_y}{E} + \frac{t-c}{R} + \frac{S_y}{E} - \frac{c}{R}\right) \tag{A.78}$$

Simplifying Equation (A.78) yields:

$$\sigma'_m = \frac{E}{2}\left(\frac{2S_y}{E} + \frac{t-2c}{R}\right) = S_y + \frac{E}{2R}(t-2c) \tag{A.79}$$

Similarly, a pseudo elastic structural bending stress can be obtained:

$$\sigma'_b = \frac{\sigma'_o - \sigma'_i}{2} = \frac{E\varepsilon_o - E\varepsilon_i}{2} \tag{A.80}$$

Substituting Equations (A.75) and (A.76) into Equation (A.80) yields:

$$\sigma'_b = \frac{E}{2}\left(\frac{S_y}{E} + \frac{t-c}{R} - \frac{S_y}{E} + \frac{c}{R}\right) \tag{A.81}$$

Simplifying Equation (A.81) yields:

$$\sigma'_b = \frac{Et}{2R} \tag{A.82}$$

A.2. Two-Sided Yielding Condition

From the requirement of equilibrium of the internal stress with the external stress, the balance of forces yields, from Figure A.3:
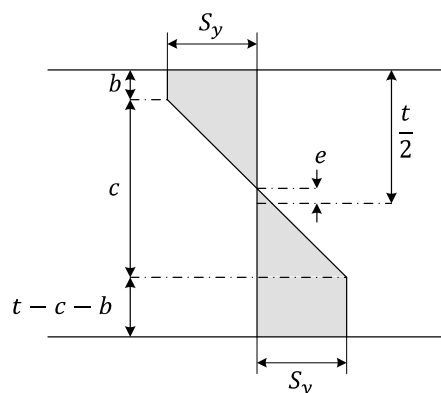
Figure A.3. Schematic of the two sided yielding condition.

$$\sigma_m t = (t - b - c)S_y - bS_y \tag{A.83}$$

Solving Equation (A.83) for c yields:

$$c = t - \frac{\sigma_m t}{S_y} - 2b \tag{A.84}$$

Similarly, taking moments about the inner surface, in reference to Figure A.3, the balance of moments yields:

$$\frac{\sigma_b t^2}{6} = \sigma_m t \left(\frac{t}{2}\right) + \frac{c^2 S_y}{6} - (t - b - c)^2 \frac{S_y}{2} + bS_y \left(t - b + \frac{b}{2}\right) \tag{A.85}$$

Simplifying and rearranging Equation (A.85) yields:

$$\frac{\sigma_b t^2}{6} = \frac{\sigma_m t^2}{2} + \left(t - \frac{\sigma_m t}{S_y} - 2b\right)^2 \frac{S_y}{6} - \left(t - b - t + \frac{\sigma_m t}{S_y} + 2b\right)^2 \frac{S_y}{2} + bS_y \left(t - \frac{b}{2}\right) \tag{A.86}$$

Expanding Equation (A.86) yields:

$$\frac{\sigma_b t^2}{6} = \frac{\sigma_m t^2}{2} + \left(t^2 - \frac{\sigma_m t^2}{S_y} - 2bt - \frac{\sigma_m t^2}{S_y} + \left(\frac{\sigma_m t}{S_y}\right)^2 + \frac{2b\sigma_m t}{S_y} - 2bt + \frac{2b\sigma_m t}{S_y} + 4b^2\right)\frac{S_y}{6}$$
$$- \left(b^2 + \frac{2b\sigma_m t}{S_y} + \left(\frac{\sigma_m t}{S_y}\right)^2\right)\frac{S_y}{2} + bS_y t - \frac{b^2 S_y}{2} \tag{A.87}$$

Rearranging and simplifying Equation (A.87) yields:

$$\frac{\sigma_b t^2}{6} = \frac{\sigma_m t^2}{2} + \frac{S_y t^2}{6} - \frac{\sigma_m t^2}{6} - \frac{S_y bt}{3} - \frac{\sigma_m t^2}{6} + \frac{\sigma_m^2 t^2}{6 S_y} + \frac{b\sigma_m t}{3} - \frac{S_y bt}{3} + \frac{b\sigma_m t}{3} + \frac{2 S_y b^2}{3}$$
$$- \frac{S_y b^2}{2} - b\sigma_m t - \frac{\sigma_m^2 t^2}{2 S_y} + bS_y t - \frac{b^2 S_y}{2} \tag{A.88}$$

Simplifying Equation (A.88) further yields:

$$\frac{\sigma_b t^2}{6} = \frac{\sigma_m t^2}{6} + \frac{S_y t^2}{6} + \frac{S_y bt}{3} - \frac{\sigma_m^2 t^2}{3 S_y} - \frac{b\sigma_m t}{3} - \frac{S_y b^2}{3} \tag{A.89}$$

Multiplying Equation (A.89) through by 6 and rearranging yields:

$$\sigma_b t^2 - \sigma_m t^2 - S_y t^2 + \frac{2\sigma_m^2 t^2}{S_y} = 2 S_y bt - 2b\sigma_m t - 2 S_y b^2 \tag{A.90}$$

that is equivalent to:

$$\frac{\sigma_b t^2}{2S_y} - \frac{\sigma_m t^2}{2S_y} - \frac{t^2}{2} + \frac{\sigma_m^2 t^2}{S_y^2} = -\left(b - \left(\frac{t}{2}\right)\left(1 - \frac{\sigma_m}{S_y}\right)\right)^2 + \frac{t^2}{4} - \frac{\sigma_m t^2}{2S_y} + \frac{\sigma_m^2 t^2}{4S_y^2}$$
(A.91)

Simplifying Equation (A.91) yields:

$$\frac{\sigma_b t^2}{2S_y} - \frac{3t^2}{4} + \frac{3\sigma_m^2 t^2}{4S_y^2} = -\left(b - \left(\frac{t}{2}\right)\left(1 - \frac{\sigma_m}{S_y}\right)\right)^2$$
(A.92)

Rearranging Equation (A.92) and solving for b yields:

$$\left(b - \left(\frac{t}{2}\right)\left(1 - \frac{\sigma_m}{S_y}\right)\right)^2 = \frac{3t^2}{4} - \frac{3\sigma_m^2 t^2}{4S_y^2} - \frac{\sigma_b t^2}{2S_y}$$
(A.93)

$$\left(b - \left(\frac{t}{2}\right)\left(1 - \frac{\sigma_m}{S_y}\right)\right) = t\sqrt{\frac{3}{4} - \frac{3\sigma_m^2}{4S_y^2} - \frac{\sigma_b}{2S_y}}$$
(A.94)

$$b = \left(\frac{t}{2}\right)\left(1 - \frac{\sigma_m}{S_y}\right) + t\sqrt{\frac{3}{4} - \frac{3\sigma_m^2}{4S_y^2} - \frac{\sigma_b}{2S_y}}$$
(A.95)

Substituting Equation (A.95) into Equation (A.84) and solving for c yields:

$$c = t - \frac{\sigma_m t}{S_y} - 2\left(\frac{t}{2}\right)\left(1 - \frac{\sigma_m}{S_y}\right) + 2t\sqrt{\frac{3}{4} - \frac{3\sigma_m^2}{4S_y^2} - \frac{\sigma_b}{2S_y}}$$
(A.96)

Simplifying Equation (A.96) yields:

$$c = t - \frac{\sigma_m t}{S_y} - t + \frac{\sigma_m t}{S_y} + t\sqrt{3 - 3\frac{\sigma_m^2}{S_y^2} - 2\frac{\sigma_b}{S_y}}$$
(A.97)

$$c = t\sqrt{3 - 3\frac{\sigma_m^2}{S_y^2} - 2\frac{\sigma_b}{S_y}}$$
(A.98)

As an aside, to determine the shift of the neutral axis of bending, e, we can also use the balance of forces:

$$\sigma_m t = S_y\left(\frac{t}{2} - \left(\frac{c}{2} - e\right)\right) - S_y\left(\frac{t}{2} - \frac{c}{2} - e\right)$$
(A.99)

Expanding Equation (A.99) yields:

$$\sigma_m t = \frac{S_y t}{2} - \frac{S_y c}{2} + S_y e - \frac{S_y t}{2} + \frac{S_y c}{2} + S_y e = 2 S_y e \tag{A.100}$$

Solving Equation (A.100) for e yields:

$$e = \frac{\sigma_m t}{2 S_y} \tag{A.101}$$

The elastic core is assumed to dominate the through-thickness deformation behavior, and so the radius of curvature is equal to the ratio of the strain in the elastic core to $c/2$, as illustrated in Figures A.3:

$$\frac{1}{R} = \frac{\varepsilon}{y} = \frac{\dfrac{S_y}{E}}{\dfrac{c}{2}} \tag{A.102}$$

Simplifying yields:

$$\frac{1}{R} = \frac{2 S_y}{c E} \tag{A.103}$$

Structural Strain at the outer and inner surface can be determined using linear extrapolation, from Figure A.3:

$$\varepsilon_o = \frac{1}{R}\left(e + \frac{t}{2}\right) \tag{A.104}$$

$$\varepsilon_i = \frac{1}{R}\left(e - \frac{t}{2}\right) \tag{A.105}$$

From the strains at the outer and inner surface, a pseudo elastic structural membrane stress can be obtained:

$$\sigma_m' = \frac{\sigma_o' + \sigma_i'}{2} = \frac{E \varepsilon_o + E \varepsilon_i}{2} \tag{A.106}$$

Substituting Equations (A.101), (A.104) and (A.105) into (A.106) yields:

$$\sigma_m' = \frac{E}{2R}\left(e + \frac{t}{2} + e - \frac{t}{2}\right) = \frac{E}{R} e = \frac{E \sigma_m t}{2 R S_y} \tag{A.107}$$

Similarly, a pseudo elastic structural bending stress can be obtained:

$$\sigma_b' = \frac{\sigma_o' - \sigma_i'}{2} = \frac{E \varepsilon_o - E \varepsilon_i}{2} \tag{A.108}$$

Substituting Equations (A.101), (A.104) and (A.105) into Equation (A.108) and simplifying yields:

$$\sigma_b' = \frac{E}{2R}\left(e + \frac{t}{2} - e + \frac{t}{2}\right) = \frac{Et}{2R} \tag{A.109}$$

References

[1] Osage, D.A., "Fatigue Assessment for In-Service Components – A New Part for API 579-1/ASME FFS-1 Fitness-For-Service," 6th Fatigue Design conference, Fatigue Design 2015, Procedia Engineering, Volume 133, 2015, Pages 320-347.

[2] Stenta, A., Gassama, E., Spring, D.W., Panzarella, C.H., Cochran, J.D., and Osage, D.A. Standardization of Fatigue Methods for Use in API 579-1/ASME FFS-1, WRC Bulletin 550, Welding Research Council, New York, N.Y., 2015.

[3] Pei, X and Dong, P, "A unified structural strain calculation procedure for fatigue evalaution of welded components: Part I – Methodology and Numerical Implementation," In Preperation, 2017.

[4] Dong, P., Pei, X., Xing, S. and Kim, M.H.,"A Structural Strain Method for Low-Cycle Fatigue Evaluation Of Welded Components," Proceedings of the ASME 2014 33rd International Conference on Ocean, Offshore and Artic Engineering, OMAE2014, June 8-13, San Francisco, California, USA.

[5] Osage, D.A. and Sowinski, J.S., ASME Section VIII – Division 2 Criteria and Commentary, ASME PTB-1, ASME, New York, N.Y., 2013.

[6] Fricke, W., *IIW Guideline for the Assessment of Weld Root Fatigue*, IIW-Doc. XIII-2380r3-11/XV-1383r3-11, Hamburg University of Technology (TUHH) Ship Structural Design and Analysis, Revision 3, June 2012.

[7] Hobbacher, A. *Recommendations for Fatigue Design of Welded Joints and Components*, WRC Bulletin 520, The Welding Research Council, new Yoork, N.Y., 2009.

[8] Dong, P., Hong, J.K., Osage, D.A., and Prager, M., *Master S-N Curve Method for Fatigue Evaluation of Welded Components*, WRC Bulletin 474, Welding Research Council, August, 2002.

[9] Dong, P., Hong, J.K., Osage, D.A., Dewees, D. and Prager, M., *The Master S-N Curve Method an Implementation for Fatigue Evaluation of Welded Components in the ASME B&PV Code, Section VIII, Division 2 and API 579-1/ASME FFS-1*, WRC Bulletin 523, Welding Research Council, New York, N.Y.

[10] Dong P, Hong J. A robust structural stress parameter for evaluation of multiaxial fatigue of weldments. Journal of ASTM International, Vol. 3, No. 7, p 206-222, 2007.

[11] Haagensen, P.J. "IIW's Round Robin and Design Recommendations for Improvement Methods," International Conference on Performance of Dynamically Loaded Welded Structures, IIW 50th Annual Assembly Conference, Proceedings of the Conference held in San Francisco, CA, July 14-15, 1997, The welding research council, Inc., new York, NY, pages 305-316.

[12] Draper, J., *Modern Metal Fatigue Analysis*, EMAS Publishing, Warrington, UK, 2008.

[13] Lee, Y, Barkey, M.E., and Kang, H., *Metal Fatigue Analysis Handbook, Practical Problem-Solving Techniques For Computer Aided Engineering*, Elsevier, Inc., 2012.

[14] Chaboche, J.L., "Time-Independent Constitutive Theories For Cyclic Plasticity," International Journal of Plasticity, 2(2), 1986, pp. 149-188.

[15] Dewees, D. J., "Application of Elastic-Plastic Design Data in the New ASME B&PV Code Section VIII Division 2," PVP2010-25641, pp. 99-109, ASME 2010 Pressure Vessels and Piping Conference, ASME, 2010, New York.

[16] Baumel Jr., A. and Seeger, T., *Materials Data for Cyclic Loading – Supplement 1*, Elsevier Science Publishing BV, 1987.

[17] Weil, N.A. and Rapasky, F.S., "Experience With Vessels Of Delayed-Coking Units," in Proceedings of the API Division of Refining, 1958, vol. 38, pp. 214–232.

[18] Coffin Jr., L.F., "A Study Of The Effects Of Cyclic Thermal Stresses On A Ductile Metal," Trans. Am. Soc. Mech. Eng., vol. 76, no. 6, pp. 931–950, 1954.

[19] Coffin Jr., L.F., "Design Aspects Of High-Temperature Fatigue With Particular Reference To Thermal Stresses," Trans. Am. Soc. Mech. Eng., vol. 78, no. 3, pp. 527–532, 1956.

[20] D. R. Miller, D.R., "Thermal-Stress Ratchet Mechanism In Pressure Vessels," Schenectady, New York, 1958.

[21] Miller, D.R., "Thermal-Stress Ratchet Mechanism In Pressure Vessels," J. Basic Eng. (Trans. ASME), vol. 81, no. 2, pp. 190–196, 1959.

[22] Bree, J.,"Elastic-Plastic Behaviour Of Thin Tubes Subjected To Internal Pressure And Intermittent High-Heat Fluxes With Application To Fast-Nuclear-Reactor Fuel Elements," J. Strain Anal. Eng. Des., vol. 2, no. 3, pp. 226–238, 1967.

[23] Moreton, D.N. and Ng, H.W., "Extension And Verification Of The Bree Diagram," Struct. Mech. React. Technol., vol. L, no. 10/2, p. 8, 1981.

[24] Ng, H.W. and Moreton, D.N., , "Bree Diagrams For Alternative Loading Sequences," in Engineering Approaches to High Temperature Design, B. Wilshire and D. R. J. Owen, Eds. Pineridge Press, Swansea, 1983, pp. 279–312.

[25] Ng, H.W. and Moreton, D.N., "Ratchetting Rates For A Bree Cyclinder Subjected To In-Phase And Out-Of-Phase Loading," J. Strain Anal. Eng. Des., vol. 21, no. 1, pp. 1–7, 1986.

[26] Ng, H.W. and Moreton, D.N., "Alternating Plasticity At The Surfaces Of A Bree Cylinder Subjected To In-Phase And Out-Of-Phase Loading," J. Strain Anal. Eng. Des., vol. 22, no. 2, pp. 107–113, 1987.

[27] Bradford, R. A. W., "The Bree Problem With Primary Load Cycling In-Phase With The Secondary Load," Int. J. Press. Vessel. Pip., vol. 99–100, pp. 44–50, 2012.

[28] Bradford, R. A. W., Ure, J. and Chen, H.F., "The Bree Problem With Different Yield Stresses On-Load And Off-Load And Application To Creep Ratcheting," Int. J. Press. Vessel. Pip., vol. 113, pp. 32–39, 2014.

[29] Spring, D.W., Panzarella, C and Osage, D.A., "Revisiting the Bree Diagram", Proceedings of the 2016 ASME Pressure Vessels & Piping Conference, PVP2016, July 17-21, 2016, Vancouver, BC, Canada

[30] Spring, D.W., Panzarella, C and Osage, D.A., Revisiting the Bree Diagram: Derivation and Extensions, Welding Research Council, In Preperation.

[31] Dong, P., Cao, Z., and Hong, J.K., "Low-Cycle Fatigue Evaluation Using the Weld Master S-N Curve," Proceedings of ASME PVP 2005 Conference (PVP2006-ICPVT11-93607), July, 2005, Vancouver, Canada.

[32] Scavuzzo, R.J., Srivatsan, T.S., and Lam, P.C., "Fatigue of Butt-Welded Pipe," Report 1 in Fatigue of Butt-Welded Pipe and Effect of Testing Methods, Welding Research Council Bulletin 433, July 1998

[33] Wais, E and Rodabaugh, E.C., "Investigation of torsional stress intensity factors and stress indices for girth welds in straight pipes", EPRI Report, #1006905, Palo Alto, CA, April, 2002

[34] Kyuba, H., and Dong, P., "Equilibrium-Equivalent Structural Stress Approach to Fatigue Analysis of a Rectangular Hollow Section Joint," International Journal of Fatigue, Vol. 27, 2005, pp. 85-94.

[35] Healy, B., "A Case Study Comparison of Surface Extrapolation and Battelle Structural Stress Methodologies," Proceedings of 23rd International Conference on Offshore Mechanics and Arctic Engineering, Paper No. OMAE2004-51228, Vancouver, British Columbia, Canada, June, 2004.

[36] Wang, et al, "Low Cycle Fatigue Analysis of Marine Structures, Paper No. OMAE 2006-92268, Proceedings of OMAE 2006, 25th Int. Conf. on Offshore Mechanics and Arctic Engineering, June 4-9, 2006, Hamburg, Germany.

[37] Markl, A.R.C., "Fatigue Tests of Piping Components," Transactions of the ASME, Vol. 74, 1952, pp.287-303.

[38] Dong, P. and Osage D.A., *Enhanced Procedurs for fatigue Evaluation of Wleded Componenets – A propsectus for a Joint Industry Project of the Pressure Vessel Research Council (PVRC) of the Welding reseach Council (WRC) and the Univeristy of Michigan*, https://forengineers.org/JIP.

[39] Pei, X., Wang, W., and Dong, P, "An analytical –based structural strain mehtod for low-cycle fatigue evaluation of girth welded pipes," Paper No. PVP2017-66006, Proceedings of ASME PVP 2017 Pressure Vessels & Piping Conference, July 16-20, Waikoloa, Hawaii, USA.